NAVAL POSTGRADUATE SCHOOL

MONTEREY, CALIFORNIA

THESIS

SAMPLE FABRICATION AND EXPERIMENTAL APPROACH FOR STUDYING INTERFACIAL SLIDING IN THIN FILM-SUBSTRATE SYSTEMS

by

Michael A. Burkhard

September 2006

Thesis Advisor: Indranath Dutta

Approved for public release; distribution is unlimited.

THIS PAGE INTENTIONALLY LEFT BLANK

REPORT DOCUMENTATION PAGE			Form Approved OMB No. 0704-0188
Public reporting burden for this collection of information is estimated to average 1 hour per response, including the time for reviewing instruction, searching existing data sources, gathering and maintaining the data needed, and completing and reviewing the collection of information. Send comments regarding this burden estimate or any other aspect of this collection of information, including suggestions for reducing this burden, to Washington headquarters Services, Directorate for Information Operations and Reports, 1215 Jefferson Davis Highway, Suite 1204, Arlington, VA 22202-4302, and to the Office of Management and Budget, Paperwork Reduction Project (0704-0188) Washington DC 20503.			
1. AGENCY USE ONLY *(Leave blank)*	**2. REPORT DATE** September 2006	**3. REPORT TYPE AND DATES COVERED** Master's Thesis	
4. TITLE AND SUBTITLE: Sample Fabrication and Experimental Approach for Studying Interfacial Sliding in Thin Film-Substrate Systems			**5. FUNDING NUMBERS**
6. AUTHOR(S) Burkhard, Michael A.			
7. PERFORMING ORGANIZATION NAME(S) AND ADDRESS(ES) Naval Postgraduate School Monterey, CA 93943-5000			**8. PERFORMING ORGANIZATION REPORT NUMBER**
9. SPONSORING /MONITORING AGENCY NAME(S) AND ADDRESS(ES) N/A			**10. SPONSORING/MONITORING AGENCY REPORT NUMBER**
11. SUPPLEMENTARY NOTES The views expressed in this thesis are those of the author and do not reflect the official policy or position of the Department of Defense or the U.S. Government.			
12a. DISTRIBUTION / AVAILABILITY STATEMENT Approved for public release; distribution is unlimited.			**12b. DISTRIBUTION CODE**

13. ABSTRACT (maximum 200 words)

The purpose of this thesis was to develop an experimental methodology to determine the mechanisms and kinetics of sliding at the interface between a metallic thin film and substrate. A methodology was developed and used to study interfacial sliding of aluminum films on silicon substrates and copper films on fused quartz substrates. The methodology employed a lap shear type of geometry to load the interface between the film and substrate in shear. The results of the studies were inconclusive with regard to interfacial sliding. In the case of Al-Si, the sample fabrication process increased the interfacial amplitude to an extent that the sliding rate was essentially zero. In the case of Cu-Fused Quartz, chromium film was added to the sample to aid the adhesion of Cu to fused quartz and as a result reduced the sliding rate below detectable levels.

14. SUBJECT TERMS Interfacial Sliding, Diffusional Sliding, Interfacial Creep, Thin Film Crawling			**15. NUMBER OF PAGES** 69
			16. PRICE CODE
17. SECURITY CLASSIFICATION OF REPORT Unclassified	**18. SECURITY CLASSIFICATION OF THIS PAGE** Unclassified	**19. SECURITY CLASSIFICATION OF ABSTRACT** Unclassified	**20. LIMITATION OF ABSTRACT** UL

NSN 7540-01-280-5500 Standard Form 298 (Rev. 2-89)
Prescribed by ANSI Std. 239-18

THIS PAGE INTENTIONALLY LEFT BLANK

Approved for public release; distribution is unlimited.

SAMPLE FABRICATION AND EXPERIMENTAL APPROACH FOR STUDYING INTERFACIAL SLIDING IN THIN FILM-SUBSTRATE SYSTEMS

Michael A. Burkhard
Lieutenant, United States Navy
B.S., United States Naval Academy, 1999

Submitted in partial fulfillment of the
requirements for the degree of

MASTER OF SCIENCE IN MECHANICAL ENGINEERING

from the

NAVAL POSTGRADUATE SCHOOL
September 2006

Author: Michael A. Burkhard

Approved by: Indranath Dutta,
Thesis Advisor

Anthony J. Healey
Chairman, Department of Mechanical and Astronautical Engineering

THIS PAGE INTENTIONALLY LEFT BLANK

ABSTRACT

The purpose of this thesis was to develop an experimental methodology to determine the mechanisms and kinetics of sliding at the interface between a metallic thin film and substrate. A methodology was developed and used to study interfacial sliding of aluminum films on silicon substrates and copper films on fused quartz substrates. The methodology employed a lap shear type of geometry to load the interface between the film and substrate in shear. The results of these studies were inconclusive with regard to interfacial sliding. In the case of Al-Si, the sample fabrication process increased the interfacial amplitude to an extent that the sliding rate was essentially zero. In the case of Cu-Fused Quartz, chromium film was added to the sample to aid the adhesion of Cu to fused quartz and as a result reduced the sliding rate below detectable levels.

THIS PAGE INTENTIONALLY LEFT BLANK

TABLE OF CONTENTS

THIS PAGE INTENTIONALLY LEFT BLANK

LIST OF FIGURES

LIST OF TABLES

THIS PAGE INTENTIONALLY LEFT BLANK

ACKNOWLEDGMENTS

I thank God through whom all things are possible. I thank my wife for her patience and understanding. I thank my advisor, Professor Indranath Dutta, for providing guidance and encouragement throughout this project. I thank Ramesh Guduru, Chanman Park, and Tom Christian for contributing their expertise and time. Lastly, I thank the Navy for giving me time away from ships to study and conduct research.

I would also like to acknowledge the financial support of the National Science Foundation, Division of Materials Research, for allowing the purchase of equipment and materials used in this thesis. This work was supported by NSF Grant DMR-0513874.

THIS PAGE INTENTIONALLY LEFT BLANK

I. INTRODUCTION

Metallic thin film-substrate systems are widely used in integrated circuits, optics, MEMS, solar power cells, and other engineering applications. In many of these applications the thin film-substrate system is subject to thermal transients during fabrication and service which can result in relatively large stress development in the film due to the difference in the coefficient of thermal expansion (CTE) between the film and substrate. Depending on the structure of the film and substrate, the nature of the bonds between the film and substrate, and the environment in which the system is used the thermal stress induced in the film may result in any number of accommodation mechanisms including elastic deformation, plastic flow, creep, crawling, sliding, delamination, or void formation to name a few.

Numerous studies on the response of metallic films to thermal transients have been conducted in the past. Many of these studies were substrate curvature tests in which specimens consisting of a relatively thick substrate coated on one side with a thin metallic film were subjected to temperature transients. Due to the typically large CTE of the metallic film and the relatively small CTE of the substrate any increase in temperature resulted in the development of a compressive stress state in the film and an overall change in curvature of the film/substrate system. Conversely, a decrease in temperature resulted in development of tensile stress in the film and curvature change in the opposite direction. The change in substrate curvature was typically measured using a laser scanning method, and the stress in the film was computed based on substrate curvature using a relation such as the Stoney equation [1]. During these experiments as temperature was varied from low to high and back to low the substrate was observed to undergo a characteristic cycle in which the film underwent elastic and plastic deformation to accommodate the thermal stresses.

The models developed to describe the response of thin films to thermal transients during substrate curvature tests usually did not account for the effect of sliding between the film and substrate. In order for sliding to occur, a shear stress had to be developed between the film and substrate. In substrate curvature experiments, the film covered a

relatively large area and appreciable shear stress was only developed at the extreme edges of the film [2,3]. Consequently only a very small percentage of the total film/substrate interface was loaded in shear and could slide. As a result, sliding had a negligible effect on substrate curvature and was excluded from models with little error.

However, in contrast to the substrate curvature experiments described above, if the in-plane film dimension (length or width) of the film was dramatically reduced to the order of the film thickness not only would the edges of the film be subject to shear loads but the entire interface between the film and substrate could be placed in a state of shear when subjected to a thermal transient. Accordingly, sliding would take on a much more prominent role in the stress development and deformation response of the films to temperature change.

In fact, experimental studies on thin films in integrated circuits and other small-area films have shown that film sliding does occur as a result of thermal transients. Out-of-plane deformation of thin film interconnects in integrated circuits was shown to be accommodated by interfacial sliding which resulted in changes in the relative heights of the interconnects and surrounding materials [4,5]. Additionally, in-plane sliding was observed in small-area aluminum films on silicon substrates resulting in in-plane dimensional changes of the films with no debonding from the substrates [3].

All things considered, interfacial sliding may become an increasingly prominent reliability consideration for microelectronics with the push for higher performing devices since a requisite for higher performance is a reduction in size of the thin film interconnects. Consequently it is important to develop a method of testing the interfacial sliding characteristics of metal films in order to better understand the mechanisms of interfacial sliding and how material and interface properties affect sliding.

II. BACKGROUND

The creep behavior of interfaces in metal-matrix composites was studied by J. V. Funn and I. Dutta [6]. In their study lead-nickel and lead-quartz single fiber composites were fabricated and subsequently tested using a fiber push down creep test. The test setup allowed the authors to isolate the interface between the fiber and matrix and load it in shear. The results of the study revealed that the interfaces in both of their composites displayed characteristics of diffusional creep with a threshold stress that decreased with increasing temperature.

Funn and Dutta interpreted the results of their single fiber composite experiments by developing a model for diffusion-controlled interfacial sliding based on Raj and Ashby's [7] continuum grain boundary sliding model. Funn and Dutta made some minor alterations to the Raj and Ashby model to account for normal stresses developed at the interfaces between fibers and matrix due to the radial thermal expansion mismatch and Poisson effect between the fibers and matrix. They also made alterations to account for the differences in diffusivity on the matrix and fiber sides of the interface. Funn and Dutta showed that the phenomena observed in their experimental data (relatively low activation energy, stress exponent equal to one, and threshold stress) were well accounted for by their model, and they concluded that their "fiber-matrix interfaces undergo thermally activated sliding via *diffusion-controlled* diffusional creep."

The model developed by Funn and Dutta to describe the kinetics of interfacial creep was:

$$\dot{\bar{U}} = \frac{2D_m^{eff}\Omega\lambda}{kT\pi h^2}\left[\tau_i + \sigma_R\left(\frac{\pi h}{\lambda}\right)^3\right] + \frac{4\delta_i D_i \Omega}{kTh^2}\left[\tau_i + 2\sigma_R\left(\frac{\pi h}{\lambda}\right)^3\right] \quad \textbf{Equation 1}$$

Where $\dot{\bar{U}}$ is the average interfacial displacement rate, D_m^{eff} and D_i are the effective matrix and interface diffusivities, Ω is the atomic volume of the diffusing species, λ is the periodicity of the interface, δ_i is the interface thickness, h is twice the interface amplitude, k is the Boltzmann constant, T is the absolute temperature, τ_i is the

shear stress applied to the interface, and σ_R is the normal (radial) stress acting on the interface. Assumed in the derivation of this model was that the interface between the fiber and matrix could be modeled such that the topography of the interface was a cosine function of the position along the interface given by:

$$x = \frac{h}{2}\cos\left(\frac{2\pi}{\lambda}y\right) \quad \textbf{Equation 2}$$

Where x is the height of the interface, h is twice the amplitude of the interface, λ is the periodicity of the interface, and y is the position along the length of the interface. Figure 1 is a schematic of the assumed topography of the interface used to derive Equation 1. Included in Figure 1 is an applied interface shear stress, τ, and the local normal stress (σ in Figure 1), which is a resultant of the applied shear stress and is shown to vary between compression and tension with the period of the interface.

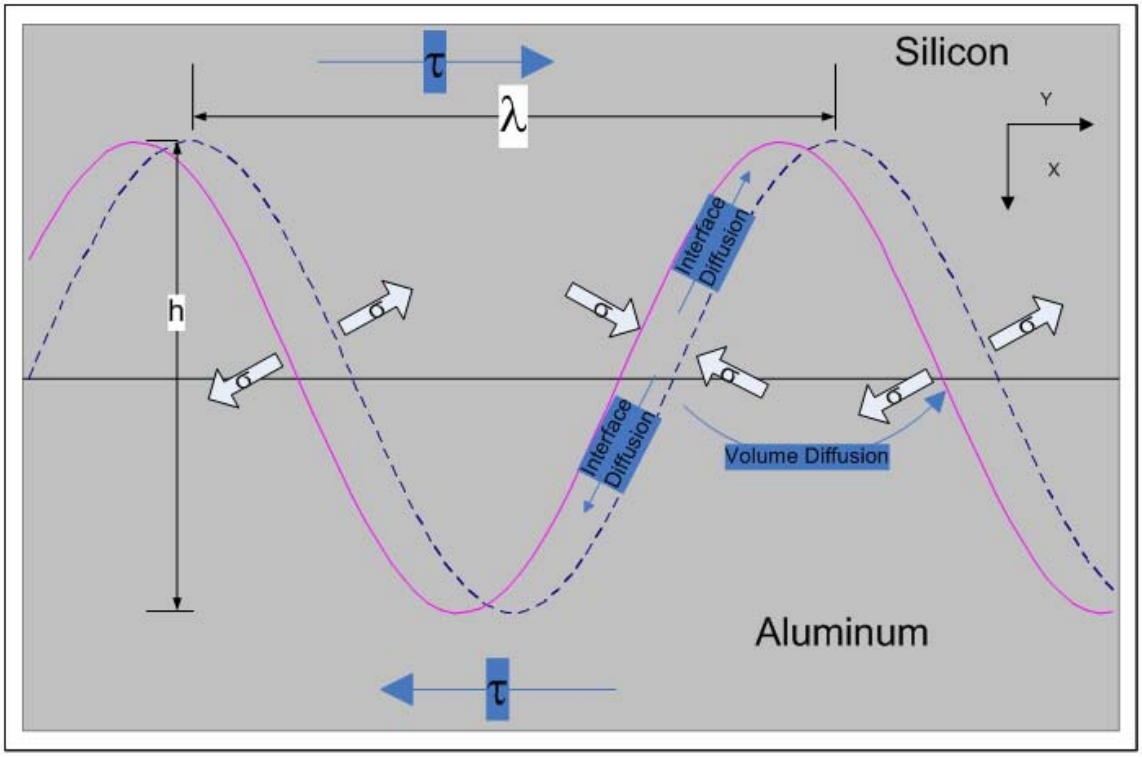

Figure 1 Schematic of the Assumed Topography of an Interface for the Derivation of Equation 1. It Includes an Applied Shear Stress and the Resultant Local Tensile and Compressive Stresses at the Interface (After Ref. [6] and [7].)

The variation between tension and compression of the local normal stress is what drives diffusion of atoms (or vacancies) at the interface and results in relative displacement between the materials on either side of the interface. Under the applied shear stress in Figure 1, Funn and Dutta's model shows that the silicon in Figure 1 would move to the right at a steady state rate, $\dot{\bar{U}}$. After a time, Δt, the Al/Si interface would move an amount $\dot{\bar{U}}\Delta t$ from the interface represented by the solid line to the interface represented by the dotted line.

Equation 1 may be simplified if $D_m^{eff} \ll D_i$. The simplified form of Equation 1 is:

$$\dot{\bar{U}} \approx K\left[\tau_i + \tau_o\right] \quad \textbf{Equation 3}$$

Where: $$K = \frac{4\delta_i \Omega D_{i_o} e^{\frac{-Q_i}{RT}}}{kTh^2}$$

$$\tau_o = 2\sigma_R \left(\frac{\pi h}{\lambda}\right)^3$$

D_{i_o} is the interfacial diffusion preexponent, Q_i is the activation energy for interfacial diffusion, and *R* is the gas constant.

Equation 3 above clearly shows that a compressive normal stress, σ_R, makes τ_o negative which implies that τ_i would need to be greater than zero to produce a positive interfacial displacement rate. As a result, a compressive σ_R is considered to result in a threshold stress type of behavior in creep of the interface. Additionally, Equation 3 shows that the effect of the interfacial roughness, as determined by the interfacial amplitude term *h*, may have an extremely large effect on the sliding rate. Very smooth interfaces are expected to have appreciable sliding rates due to the presence of h^2 in the denominator.

In a separate study Peterson, Dutta, and Chen [8,9] found that interfaces in bulk diffusion bonded Al-Si samples slide by "interface diffusion-controlled" diffusional creep. In their work, experiments were devised in which three of the major components

in the model proposed by Funn and Dutta and given in Equation 1 above; interfacial shear stress (τ_i), normal stress (σ_R), and interfacial roughness (*h*), could be varied independently and tested to determine their effect on interfacial sliding. Testing was performed by heating a test specimen to a high homologous temperature, mechanically loading the Al-Si interface, and observing the relative displacement of the aluminum and silicon. Relative displacement was measured using a non-contact capacitance gauge and found to be nearly entirely accommodated by sliding at the interface between the Al and Si. An apparent activation energy and stress exponent for interfacial creep were determined to be Q = 42 kJ/mol and n =1. A temperature independent threshold stress was determined to exist when a normal stress (σ_R) was applied to the interface and vanish when the normal stress was removed. The interfacial displacement rate was found to be proportional to $\frac{1}{h^2}$. Based on the relatively low activation energy, the stress exponent, the existence of a threshold stress, the displacement rate dependence on $\frac{1}{h^2}$, and microstructural evidence the authors concluded that the interface underwent "interface diffusion-controlled" diffusional creep and that its behavior was well described by Funn and Dutta's interfacial sliding model.

In addition to the interfaces between the fibers and matrices in certain metal matrix composites and Al-Si diffusion bonded interfaces, interfacial sliding has also been observed in several thin film systems. Zhmurkin, Gross, and Buchwalter [5] studied high density interconnect structures (HDICs) and observed out of plane interfacial sliding between copper interconnects and tantalum liners as a result of differences in thermal expansion. In this study the authors used atomic force microscopy to observe out of plane deformation in HDICs before and after subjecting them to a thermal cycle between room temperature and 350^{o}C. From their observations, the authors concluded that some of the deformation they observed was a result of diffusionally accommodated interfacial sliding between the copper interconnects and tantalum liners. Gross, Kamash, and Tsukrov [10], extended Zhmurkin et al.'s work by generating out-of-plane deformation maps of Cu-polyimide damascene interconnect structures using scanning probe

microscopy and also provided evidence of interfacial sliding between copper interconnects and tantalum liners. Park, Dutta, Peterson, and Vella [4] performed similar atomic force microscopy studies on thermally cycled standalone thin film copper lines on silicon, and thermally cycled thin film copper/low k dielectric structures on silicon. Park et al. observed both out-of-plane interfacial sliding as well as in-plane interfacial sliding at copper/tantalum interfaces as a result of thermal cycling.

In addition to the observations of thin film copper interfacial sliding noted above, Dutta and Chen [3] provided evidence of in plane interfacial sliding between aluminum thin films and silicon substrates as a result of thermal cycling. Using atomic force microscopy, they measured the in-plane dimensions of relatively small (6μm x 6μm) area films before and after thermal cycling. After several thermal cycles, they found the films had accumulated large in-plane permanent strains; however, these strains were found to be larger near the Al-Si interface than at the free surface of the films. Dutta and Chen attributed this phenomena to a through thickness gradient of in-plane stress where the maximum stress occurred at the Al-Si interface and was accommodated by interfacial sliding between the Al and Si.

In yet another study, Moiré interferometry was used to measure the interfacial behavior of model flip-chip structures subject to thermal transients [11]. The flip-chips consisted of a silicon chip bonded to an FR4 substrate with a layer of underfill epoxy. The interfaces studied were the silicon/epoxy and epoxy/FR4 substrate interfaces. Moiré interferometry was used to measure the relative displacements of the layers in the flip-chips while the chips were subject to thermal cycles with various temperature vs. time profiles. From the displacement data, the evolution of shear strain and strain recovery were determined and concluded to be a result of creep processes at the interfaces.

Typically, when a large area thin film is subject to a thermal transient only the edges of the film are actually subject to the shear loading that may give rise to interfacial sliding [2,3]. However, when the in plane dimensions of the film are scaled down to the order of the thickness of the film, a large percentage of the interface can be subject to shear loading making interfacial sliding an important factor in the deformation characteristics of the film. This is the case in most of the thin film studies mentioned

above. In addition to shear loading resulting from the difference in thermal expansion between the film and its underlying substrate, shear loading which may result in sliding can also result from far field stresses applied to the film as a result of loads imposed by packaging in microelectronic applications. This condition may be exacerbated when the package is subjected to thermal cycles causing the films to crawl across their substrates in small increments [12,13].

As mentioned in the preceding paragraphs, sliding at interfaces in the metal matrix composites of Funn and Dutta and the diffusion bonded Al/Si samples of Peterson et al. has clearly been characterized and shown to be compatible with the interface diffusion-controlled diffusional creep model. Interfacial sliding has also been observed in numerous studies on thin films. However, the thin film studies did not provide evidence of the time dependent mechanisms or kinetics which accommodated sliding. The focus of this thesis is to develop an experimental approach to determine the mechanisms and kinetics of sliding in a representative thin film system.

III. OBJECTIVE

The objective of this research was to develop an experimental methodology to determine the mechanisms and kinetics of sliding at the interface between a thin metallic film and substrate. The approach to achieve this objective was several-fold. The first step was to develop a specimen and mechanical test which permitted the in situ measurement of interfacial sliding. The second step was to fabricate the specimen and testing apparatus, and the final step was to use the mechanical test to gather experimental data about the mechanisms and kinetics of interfacial sliding.

THIS PAGE INTENTIONALLY LEFT BLANK

IV. EXPERIMENTAL PROCEDURE

The experimental procedure consisted of two major steps, sample fabrication and mechanical testing. The sample geometry was adopted from work done by Naval Postgraduate School students Mark Thornell and Carl Parks [14,15]. Figure 2 is a schematic of the sample geometry. The sample consisted of a thin metallic film sandwiched between two rigid and relatively refractory substrates. Grooves were cut in the two substrates to form a lap shear type of geometry, also depicted in Figure 2, in which a globally applied compressive load resulted in shear loading of the thin film/substrate interface.

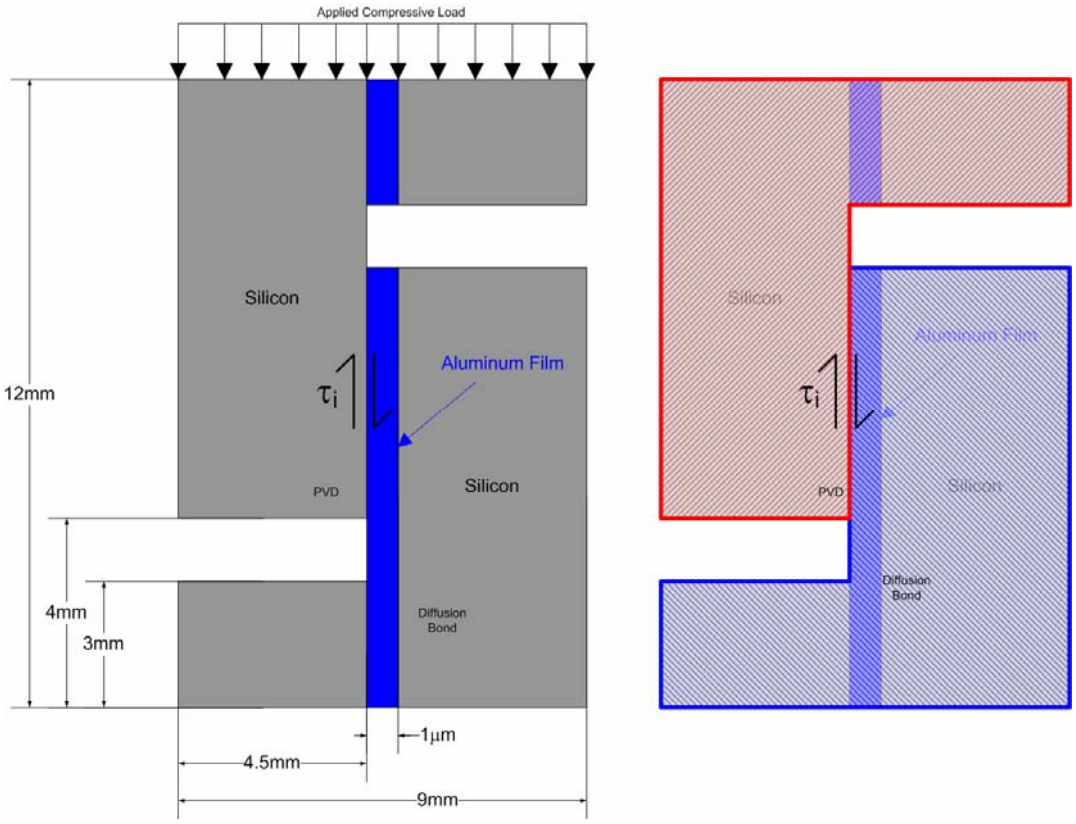

Figure 2 A Schematic of an Al/Si Sample with Approximate Dimensions (Not to Scale) and Applied Loads. The Two Halves of the Lap Shear Geometry are Highlighted in the Figure to the Right.

Samples with two different sets of materials were tested. The first consisted of silicon substrates and aluminum film, which are referred to as Al/Si samples throughout the rest of the paper. The other samples consisted of fused quartz substrates and copper film and are referred to as Cu/Quartz samples.

Sample fabrication is detailed in the sections that follow (Materials, Film Deposition, Diffusion Bonding, and Etching) and generally consisted of the following steps for Al/Si samples: The first was to obtain lapped and well polished substrates, then to deposit a thin metallic film by physical vapor deposition on one side of one substrate. The next step was to form a diffusion bond between the thin film on one substrate and the bare surface of another substrate to form the substrate/thin film/substrate sandwich structure. After diffusion bonding, the sandwich structure was cut to the desired dimensions (12mm x 9mm x 6mm), and the two grooves that formed the lap shear halves were cut. After cutting the grooves, the samples were etched to extend the grooves up to but not through the metallic film as described in the etching section.

In Figure 2, the interface between the Si substrate and the Al film that was formed during film deposition is labeled “PVD” whereas the interface formed by diffusion bonding is labeled “Diffusion Bond.” Figure 2 also highlights the two halves of the lap shear geometry with cross hashes. The union between the two halves of the lap shear specimen is at the “PVD” interface. As noted above the grooves in the specimen were extended up to but not through the metallic film by chemical etching. In order to isolate the PVD interface for testing, the upper groove depicted in Figures 2 was further extended, through the metallic film, by sanding with silicon carbide polishing paper until the film at the end of the groove was completely removed. In so doing the “PVD” interface could be loaded in shear and sample deformation could be relatively isolated to the “PVD” interface.

The Cu/Quartz sample fabrication procedure deviated slightly from the Al/Si procedure. Instead of depositing film on only one substrate and forming a diffusion bond between the film and a bare substrate as in the Al/Si samples, Cu film was deposited on two separate substrates, and a diffusion bond was formed between the two Cu films. Since no chemical etch was available to selectively etch quartz and not copper, the

notches in the samples were cut such that both extended through the film. Figure 3 is a schematic of a typical Cu/Quartz sample.

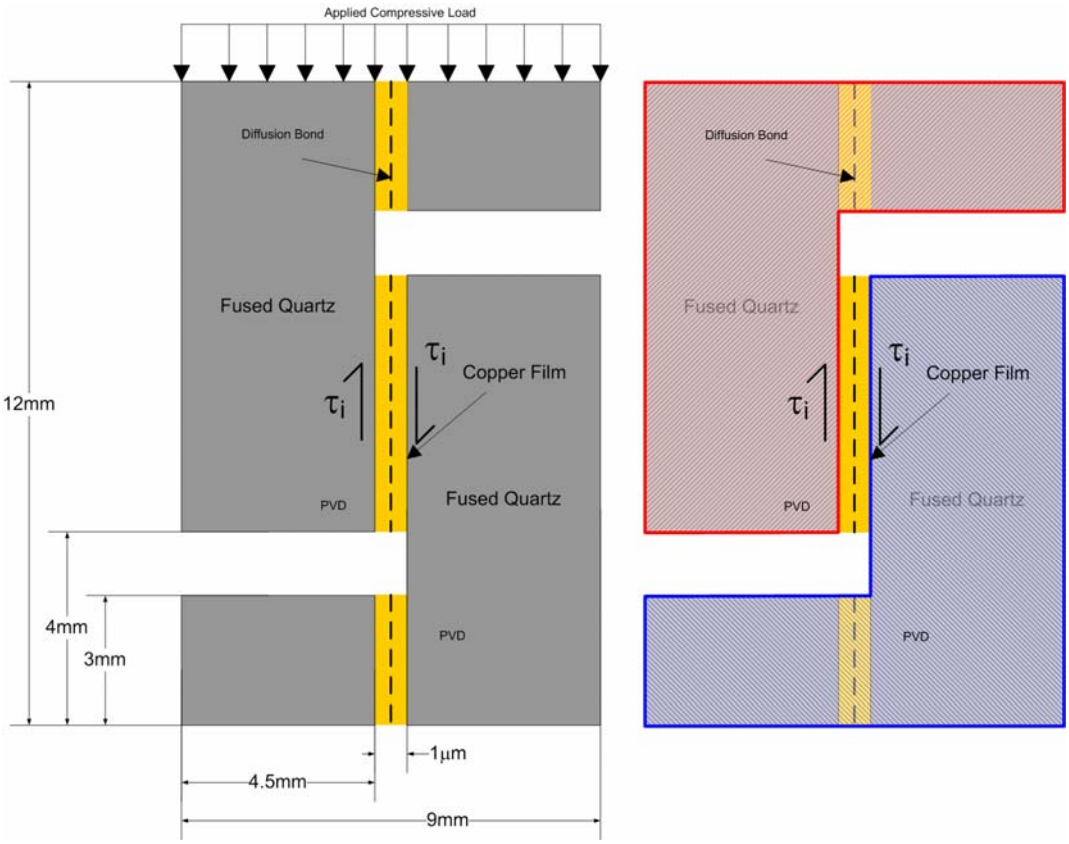

Figure 3 A Schematic of a Cu/Quartz Sample with Approximate Dimensions (Not to Scale) and Applied Loads. The Two Halves of the Lap Shear Geometry are Highlighted in the Figure to the Right.

A major difference between the Al/Si samples and the Cu/Quartz samples, which is highlighted in Figure 3, was that by extending both grooves through the film, the test section of the film was not incorporated into either of the lap shear halves as it was in the Al/Si samples. As a result, both of the substrate/film interfaces could slide and the film could more easily deform in shear in the Cu/Quartz samples.

Mechanical testing is detailed in the section titled "testing," and it generally consisted of heating the specimen to a high homologous temperature and applying a

compressive load to the specimen. To determine interfacial deformation, the relative displacement of the two halves of the lap shear geometry was measured.

A. MATERIALS

1. Substrates

An undoped single crystal silicon ingot with {100} orientation was procured from Virginia Semiconductor. This ingot was sectioned into 28mm x 28mm x 4.5mm blocks which were subsequently lapped and polished by Valley Design. Polished fused quartz substrates, 25mm x 25mm x 3mm, were procured from Goodfellow and, 25mm x 25mm x 4.5 mm, fused quartz substrates were procured from Valley Design.

The silicon substrates were prepared for film deposition by cleaning with a series of organic solvents, deionized water, and dilute HF acid. The first two solvents used were acetone and 2 – propanol. The substrates were first degreased with acetone in an ultrasonic tank and rinsed with deionized water. Afterward, they were further degreased with 2-propanol in the ultrasonic tank and again rinsed with deionized water. Next the substrates were immersed in 10wt% HF acid for 45 seconds followed by a rinse with deionized water. The purpose of the acid immersion was to remove any native silicon oxide and metallic contaminants from the silicon. After the acid immersion, the substrates were rinsed one last time with deionized water and blown dry with nitrogen.

The fused quartz substrates were also prepared by cleaning with a series of organic solvents, and deionized water; however, they were not exposed to any acid. The fused quartz was first degreased with acetone in an ultrasonic tank at room temperature for 5 minutes. This was followed by a rinse in acetone at approximately 40^{o}C for 10 minutes, which was followed by a rinse in a bath of methanol also at approximately 40^{o}C but for only 5 minutes. After the acetone and methanol baths, the fused quartz substrates were rinsed in room temperature deionized water in an ultrasonic tank for 5 minutes. They were then removed from the tank and given a final rinse with flowing deionized

water; after which the substrates were immediately blown dry with compressed nitrogen. It was found that this procedure resulted in a clean grease free surface with virtually no residue from the organic solvents.

2. Film Deposition Material

High purity aluminum shot (99.9%) was procured from Sigma Aldrich for deposition on the silicon substrates. The aluminum shot was prepared for deposition by cutting it into small, approximately 2mm diameter, pieces. High purity copper shot (99.9999%) was procured from Goodfellow for deposition on the fused quartz substrates. The copper shot was loaded into the film deposition system as received. Lastly, a small amount of chromium was used along with the copper on the fused quartz substrates. It was procured from Ernest F. Fullam, was 99.9% pure, and came in the form of chips.

B. FILM DEPOSITION

All metal film deposition was performed by thermal evaporation in a diffusion pumped vacuum chamber with a vacuum of approximately $1x10^{-7}$ torr.

1. Aluminum Film

First, a clean silicon substrate was loaded in a substrate holder, and aluminum deposition material was loaded in tungsten baskets. The aluminum and silicon were then inserted in the vacuum chamber and high vacuum was drawn. Next, the silicon substrate was baked at a temperature of $200^{o}C$ for an hour to help release any residual moisture and other volatiles adsorbed on the substrate surface. After baking the substrate, film deposition was carried out by passing current through one of the tungsten baskets containing aluminum thereby heating and evaporating the aluminum. Aluminum film deposition was controlled at a rate of approximately 1nm/sec until the desired film thickness was achieved by varying the current to the tungsten basket. It was found that between 27 and 30 amps resulted in approximately 1nm/sec deposition rate. Due to the limited quantity of aluminum in each tungsten basket and the affinity of the tungsten baskets for alloying with aluminum and subsequently breaking, often times it was

necessary to use more than one basket of aluminum to achieve the desired film thickness. The film thickness was measured using a Cressington MTM-10 in situ film thickness monitor.

After completing deposition, the substrates were cooled to room temperature in vacuum prior to removal from the deposition system.

2. Copper Film

Copper films were deposited in a similar manner to the aluminum film described above. A clean fused quartz substrate was loaded in a substrate holder, and deposition material was loaded in tungsten baskets. All of the materials were then inserted in the vacuum chamber and high vacuum was drawn. After drawing vacuum, the substrate temperature was raised to 150^{o}C and maintained for at least an hour prior to deposition to help release any moisture adsorbed on the substrate surface.

As an aside, it was found that the copper films would usually delaminate or peel from the fused quartz substrates after diffusion bonding if the copper was deposited directly on fused quartz. In order to prevent the copper from delaminating, a 10 nm thick film of chromium was deposited on the fused quartz prior to depositing copper. Chromium seemed to be extremely adhesive to fused quartz, and it significantly increased the adhesion of the copper film resulting in overall more durable samples. The effect of chromium addition on the test results is discussed in the "Results and Discussion" chapter below.

After depositing chromium, copper was immediately deposited at a rate of approximately 0.2 nm/sec. This deposition rate was achieved by passing approximately 33-35 amps of current through the tungsten basket. It was found that during film deposition the substrate temperature generally rose to approximately 265^{o}C due to radiative heating from the tungsten basket. In order to prevent a rapid decrease in substrate temperature and subsequent spalling or delamination of the copper film due to thermal shock, the substrate cool down was controlled by slowly stepping down the current to the tungsten basket and simultaneously adjusting the substrate heater current

upward to maintain substrate temperature relatively constant. This was continued until the tungsten basket current was zero and the substrate heater maintained the substrate temperature nearly constant. Afterward, the substrate heater current was slowly stepped down thereby controlling the substrate cool down rate and minimizing the thermal shock to the film and substrate.

C. DIFFUSION BONDING

Diffusion bonding was performed in a chamber mounted in a SATEC load frame. Figure 4 is a schematic of the diffusion bonding chamber and associated equipment. Al/Si and Cu/Quartz samples were prepared for diffusion bonding by stacking substrates in the appropriate sequence and sandwiching them between layers of aluminum and graphite (for the Al/Si samples) or copper and graphite (for the Cu/Quartz samples) and loading them in a die (29mm x 29mm) constructed of high carbon steel. The die and sample arrangement are depicted in Figure 5. The aluminum, copper, and graphite layers prevented cracking of the samples during loading and lubricated the surfaces preventing the samples from sticking to the die.

After loading the samples in the die, the die was inserted into the diffusion bonding chamber, and the chamber was sealed by bolting the bottom flange of the chamber to the bellows assembly depicted in Figure 4. After sealing the chamber, an argon/hydrogen atmosphere was established within the chamber, and the samples were loaded in uniaxial compression with the SATEC load frame.

Once the samples were loaded in compression, the temperature of the samples was increased at a rate of 25^{o}C/min using an external furnace controlled by a feedback temperature controller. Temperature was monitored using a K-type thermocouple mounted on the outside of the diffusion bonding chamber as depicted in Figure 4. Since the thermocouple was located outside the chamber, the actual sample temperature lagged the indicated temperature during the heat up from room temperature to diffusion bonding temperature. After reaching the desired diffusion bonding temperature, indicated by the thermocouple, temperature was held constant for the desired bonding time.

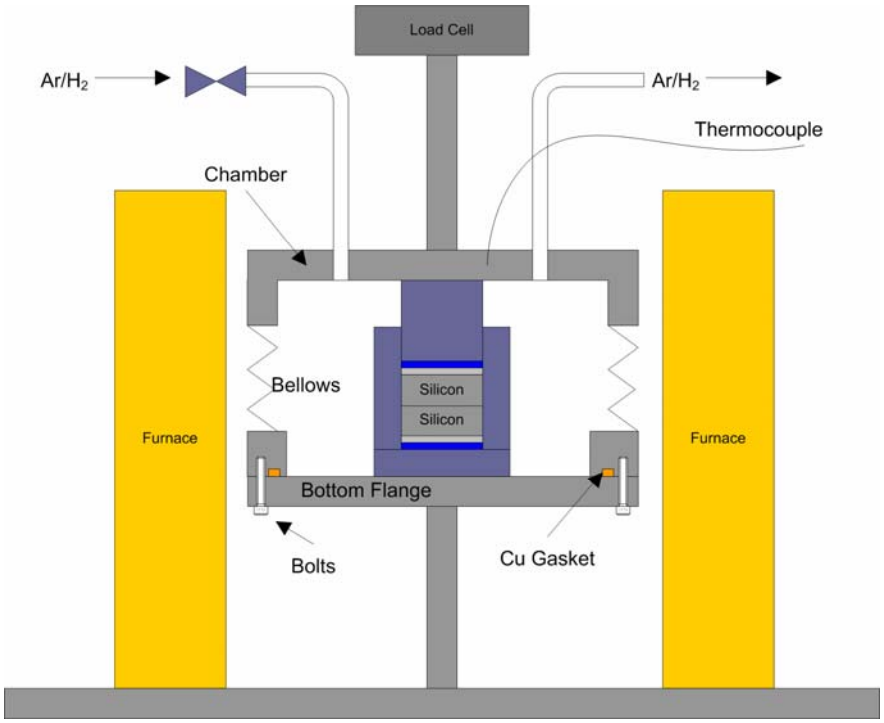

Figure 4 Diffusion Bonding Chamber Schematic

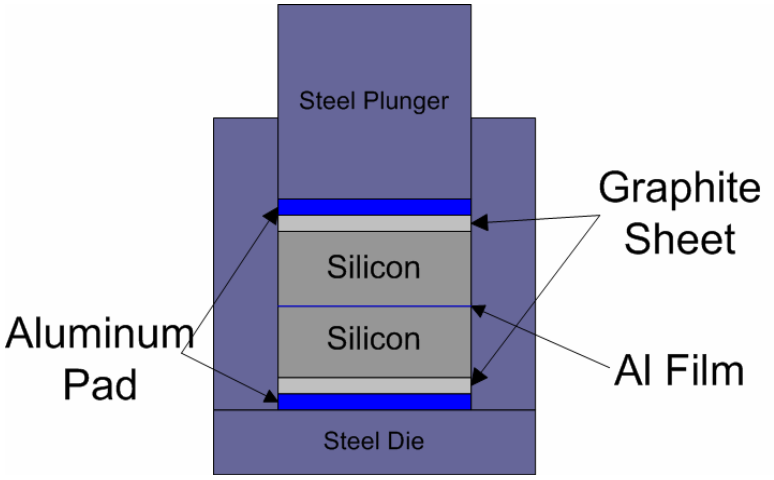

Figure 5 Diffusion Bonding Die with an Example of the Sample Orientation

During this constant temperature hold, the actual sample temperature continued to increase until reaching equilibrium at the indicated temperature. At the conclusion of the constant temperature hold the furnace was switched off and the samples were slowly

cooled over the course of many hours to room ambient temperature. Finally, after cooling to ambient temperature the load was removed from the samples, and the samples were removed from the diffusion bonding chamber by disassembling the chamber and die.

The parameters used to form diffusion bonds are listed in Table 1 and detailed in the following sections.

1. Aluminum-Silicon

As stated earlier most of the Si/Al samples were fabricated by forming a diffusion bond between a bare silicon substrate and an aluminum film that had been previously deposited on a second silicon substrate. The bonding was carried out at 550^{o}C, in a 98%Ar/2%H_2 atmosphere, for 2 hours, under 7 MPa uniaxial compressive stress. The temperature, time, and stress parameters were based on work done by Parks [15].

2. Aluminum-Aluminum

In addition to diffusion bonding Al to Si, several Al/Si samples were also fabricated by forming a diffusion bond between two aluminum films, similar to the procedure described earlier for the Cu/Quartz samples. The same parameters described in the Aluminum-Silicon section above worked well for aluminum thin film to aluminum thin film diffusion bonding. The temperature was maintained at 550^{o}C, the atmosphere was 98%Ar/2%H_2, the time was 2 hours, and 7 MPa uniaxial compressive stress was used.

It is commonly thought that forming diffusion bonds between bulk aluminum parts is difficult due to the tenacious oxide layer that aluminum forms upon exposure to air. This surface oxide layer tends to prevent the diffusion of aluminum from one component to the other resulting in little or no bonding. Many researchers have studied methods of overcoming this oxide layer using techniques such as transient liquid phase (TLP) bonding [16,17], using proprietary organic compounds to protect the bare

aluminum surfaces prior to bonding [18], or using relative motion between the aluminum components to break up the oxide layer [19].

No such difficulty was encountered in diffusion bonding the aluminum thin films to one another. Usually it was found that the diffusion bond was actually stronger than the surrounding silicon substrates. Whenever samples broke, either due to testing or inadvertently due to mishandling, the samples almost always broke by cleavage of the silicon substrate rather than along the diffusion bond.

3. Copper-Copper

The Cu/Quartz samples required the formation of a diffusion bond between two copper films. The bonding parameters used were a temperature of 650^{o}C, in a 98% Ar / 2% H_2 atmosphere, for a time of 1 hour, under 10 MPa uniaxial compressive stress. The atmosphere was established by roughing the diffusion bonding chamber with a mechanical vacuum pump to approximately 1 torr then backfilling the chamber with Ar/H_2 gas to atmospheric pressure. Roughing and backfilling were performed three times, then the vacuum connection was removed and a hose was connected to the chamber to allow Ar/H_2 gas to flow from the chamber into a bucket of water and out to atmosphere. The water was used to create a backpressure of Ar/H_2 in the diffusion bonding chamber and to prevent oxygen diffusion from the outside atmosphere back into the chamber.

Diffusion Bonding Parameters				
Sample Type	Temperature (C)	Pressure (MPa)	Time (hr)	Atmosphere
Al/Si	550	7	2	98% Ar - 2% H2
Cu/Quartz	650	10	1	98% Ar - 2% H2

Table 1 Diffusion Bonding Parameters

D. SAMPLE DICING

After diffusion bonding, the samples were cut to test size using a standard low speed diamond saw. Typically the outside edge of the substrates was poorly bonded. In order to find the region of good bonding; the sample was mounted to a glass holder with

wax and thinly sliced until a region of good bonding was reached. Upon finding the region of good bonding, the sample was sliced into as many 6mm x 12mm blocks as possible. Typically one diffusion bonded Si/Al/Si sandwich yielded three 6mm x 12mm blocks.

After cutting diffusion bonded samples into blocks, the samples were removed from the glass holder, and grooves were cut into the substrates as shown in Figure 6. For the Al/Si samples the grooves were cut as close as possible but not quite touching the aluminum film, typically within 0.1mm of the film. For the Cu/Quartz samples the grooves were made deep enough such that the Cu film was just completely cut through and no more than 0.1mm deeper.

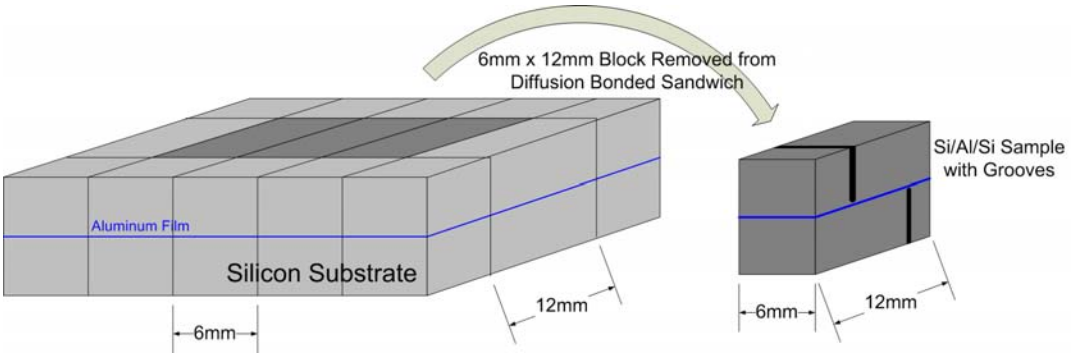

Figure 6 Schematic of a Diffusion Bonded and Diced Si/Al/Si Sandwich Specimen with a Single Sample Removed and Grooves Cut.

After cutting grooves with the diamond saw, the Al/Si samples were etched (explained in the next section) to extend the grooves to the Al film. Once the groove was extended to the Al film, SiC polishing paper was used to remove the film in the groove on the diffusion bonded side of the sample. Finally, the ends of the samples were sanded flat and the corners were beveled. Figure 7 contains photographs showing different perspectives of a completed Cu/Quartz sample.

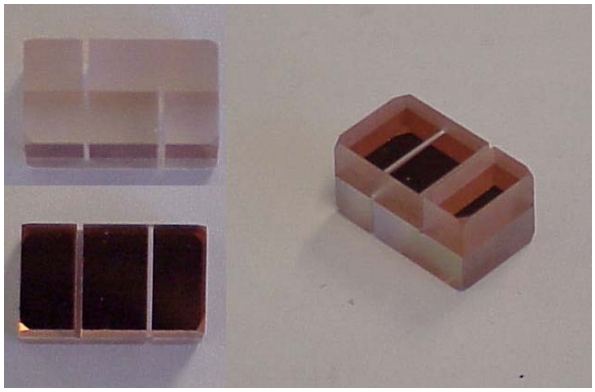

Figure 7 Photographs Depicting Several Perspectives of a Completed Cu/Quartz Sample

E. ETCHING (ALUMINUM/SILICON SAMPLES)

After dicing and cutting grooves in the Al/Si samples, the samples were placed in an etching solution capable of etching silicon but not aluminum. Using this etching solution, the sample's grooves were extended through the silicon until the bottom of the grooves reached the underlying aluminum film. After the aluminum film was reached, the sample was rinsed and the aluminum film in the notch on the diffusion bonded side of the sample was removed with polishing paper.

Tetra-methyl ammonium hydroxide (TMAH), $(CH_3)_4NOH$, was used to perform silicon etching. Used alone TMAH not only etches silicon but also rapidly etches aluminum. However, if a small amount of silicon is dissolved in the TMAH prior to attempting to etch an aluminum containing sample, a protective layer will form on any aluminum that is subsequently immersed in the solution and prevent the aluminum from being attacked by the TMAH. Typically silicon that has been etched using TMAH becomes roughened due to the selectivity of TMAH for etching {100} oriented surfaces over etching {111} oriented silicon surfaces. This selectivity results in the formation of micro-pyramids or hillocks on the surface of the silicon. In order to reduce the formation of these hillocks, an oxidizing agent such as ammonium persulfate, $(NH_4)_2S_2O_{8,}$ may be added to the TMAH [20-22].

TMAH solution was prepared by diluting stock 25wt% TMAH with deionized water to a concentration of 5wt%. Approximately 100ml of 5wt% TMAH was then

measured into a plastic beaker and warmed to 50^{o}C in a bath of heated water by suspending the beaker of TMAH in the water. To prevent excessive evaporation of the TMAH solution, the beaker was loosely covered with a concave glass cover.

Next 1.4wt% powdered silicon (approximately 1.42g Si per 100ml of 5wt% TMAH) was added to the 50^{o}C TMAH and allowed to completely dissolve. The TMAH solution was maintained at about 50^{o}C while dissolving the powdered silicon to prevent excessive bubbling and evaporation which occurs with higher temperature. The silicon was powdered by crushing small pieces of bulk silicon with a mortar and pestle. It typically took approximately 2 hours to dissolve all of the silicon.

After dissolving the silicon, the temperature of the TMAH solution was raised to 90^{o}C and 0.5wt% (approximately 0.50g per 100ml of TMAH solution) ammonium persulfate was added to the TMAH solution. After the ammonium persulfate was dissolved (approximately 20 minutes), an Al/Si sample was immersed in the TMAH solution. Temperature was maintained at 90^{o}C for the duration of etching.

An Al/Si sample was allowed to etch for up to 4 hours in the original solution before a fresh TMAH solution was prepared. The sample was occasionally removed from the TMAH solution to check the progress of etching. When aluminum film was clearly visible at the bottom of the grooves, the sample was finally removed from the TMAH solution and cleaned with water. The aluminum film appeared as a highly reflective silvery surface at the groove bottom when it was reached. Often times eight or more hours of etching were required to reach the aluminum film.

Figure 8 is an optical micrograph of the groove in an Al/Si sample prior to etching. The Al film appears as the very thin black line below the groove. Figure 9 is an optical micrograph of the same Al/Si sample after etching. From Figures 8 and 9 it is evident that the TMAH solution etched the Si and effectively extended the groove up to but not through the Al film.

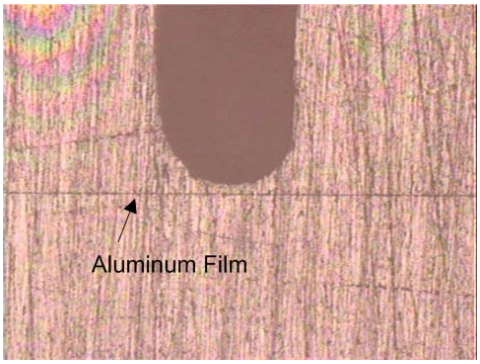

Figure 8 Optical Micrograph Showing the end of a Groove in an Al/Si Sample Prior to Etching.

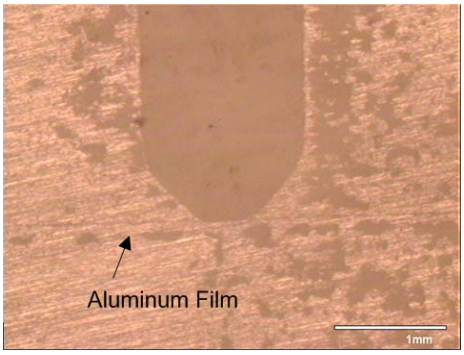

Figure 9 Optical Micrograph Showing the Same Groove as in Figure 8 After Etching.

F. TESTING

Mechanical testing consisted of three basic steps; heat the specimen to high homologous temperature, apply uniaxial compressive stress to the specimen, and measure the deformation of the specimen with respect to time.

The test apparatus consisted of an MTS servohydraulic load frame equipped with 500lbf and 2200lbf load cells, inner and outer environmental chambers, temperature feedback controlled furnace, and capacitance displacement gauge. The environmental chambers were used to minimize the effect of the laboratory environment such as ambient temperature change on the creep test results. In addition to the environmental chambers which insulated the area surrounding the furnace and specimen from the

laboratory, fiberglass insulation was wrapped around the load cells to minimize temperature change at the load cells from causing load changes due to shift of the load cell zero.

The furnace consisted of a pair of Watlow radiant strip heaters controlled by a Watlow temperature controller. The controller received a feedback signal from a thermocouple located next to the specimen in the inner environmental chamber. Using the environmental chambers, strip heaters, and temperature controller, it was possible to control temperature to within +/-0.2^{o}C of the desired setpoint.

The capacitance displacement gauge was a high temperature type with an inconel case manufactured by Capacitec. The capacitance gauge was calibrated to measure the distance between the capacitance gauge probe and a target up to 250 μm away with a resolution of <0.1μm. The probe was mounted in an inconel base plate and fixed with two set screws. The target was a tungsten rod which was mounted in a second inconel block and fixed with a set screw.

Temperature was measured at three locations using K type thermocouples. Two thermocouples were located next to the test specimen inside the inner environmental chamber; one was used for control of the furnace, and the other was used for recording and displaying sample temperature. The third thermocouple was located at the bottom of the 500lbf load cell. It was used to record and display load cell temperature.

Uniaxial compressive load was applied to the test specimen with the servohydraulic load frame using a feedback signal from the 500lbf load cell. When required to control the load frame in displacement mode, the system's linear variable differential transformer (LVDT) sensor was used to supply a displacement feedback signal.

In order to minimize any deformation of the load frame from affecting the creep test displacement data, the capacitance gauge and target were positioned to measure the actual test specimen displacement as directly as possible. The test specimen was sandwiched between two inconel blocks as shown in Figure 10. The bottom inconel block supported the bottom of the test specimen, and it was also used to mount the

capacitance gauge probe. As a result, the bottom inconel block served as the zero reference for specimen displacement. The top inconel block was used to press down and apply load to the top of the specimen. It also held the capacitance gauge target. Any displacement measured by the capacitance gauge was limited to deformation of the test specimen and the two inconel blocks. Since the deformation of the inconel blocks was expected to be extremely small at the relatively low loads and low homologous temperature (for inconel) used in testing, the measured displacement corresponded primarily to the test specimen.

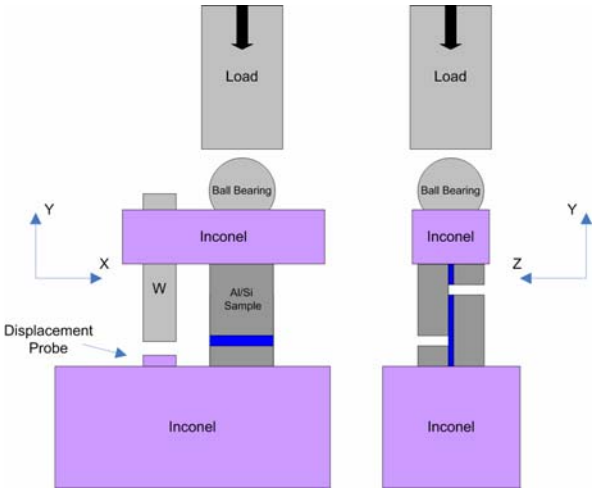

Figure 10 Schematic Showing Two Perspectives of the Test Setup.

As can be seen in Figure 10, there was a small stainless steel ball bearing set into a cylindrical cut in the top of the top inconel block. The ball bearing's purpose was to accommodate any misalignment along the y-axis of Figure 10 between the test specimen and load train and ensure the line of loading was directly down the length of the test specimen's metallic film. If the line of loading was eccentric to the length of the film, the specimen would deform by bending and compression rather than simple compression.

The general testing procedure was to place the specimen in the test apparatus, bring the capacitance displacement gauge into range, close the environmental chambers, and heat the sample to the desired test temperature with the furnace. After reaching the test temperature, a temperature soak of nine hours was performed in which the specimen

temperature was maintained constant. The soak was performed to bring the entire test apparatus to thermal equilibrium and to provide sufficient time for any stresses induced in the test specimen by the temperature transient (room temperature to the test temperature transient) to relax.

After performing the temperature soak, the test specimen was loaded in uniaxial compression using the servohydraulic load frame and held at this load for up to 72 hours. The load was controlled and maintained using a feedback signal from one of the load cells, usually the 500lbf load cell. Throughout the test data was collected from the 500lbf and 2200lbf load cells, the capacitance displacement gauge, and the thermocouples. At the completion of the test, the specimen was unloaded and then either retested at a different load or cooled to room temperature.

THIS PAGE INTENTIONALLY LEFT BLANK

V. RESULTS AND DISCUSSION

A. INTERFACIAL SLIDING

1. Test Results

The Al/Si samples were tested at stresses between 1MPa and 7MPa and temperatures between 573K and 673K for up to 12 hours. The Cu/Quartz samples were tested at stresses between 3MPa and 7MPa and temperatures between 584K and 633K for up to 72 hours. The results of these tests were inconclusive with regard to interfacial sliding. The samples exhibited extremely small total displacements that seemed to be relatively independent of load or temperature. Figures 11 and 12 are typical displacement versus time plots obtained for Al/Si and for Cu/Quartz samples respectively. Each figure shows displacement plots for three different loading and temperature conditions. In both figures, the total measured displacement was extremely small, 0.2μm for Al/Si and 0.6μm for Cu/Quartz.

The time scales in Figures 11 and 12 are different. The Cu/Quartz samples were tested for longer times to determine whether significantly larger displacement might occur with longer duration tests thereby allowing the interfacial displacement to be separated from testing error. However, with the longer duration tests and the slightly larger overall displacement an unexpected periodic oscillation in the displacement occurred. All three sets of displacement data in Figure 12 show a periodic oscillation in which the test specimen appears to go through a period of relatively rapid deformation in compression followed by a period of recovery.

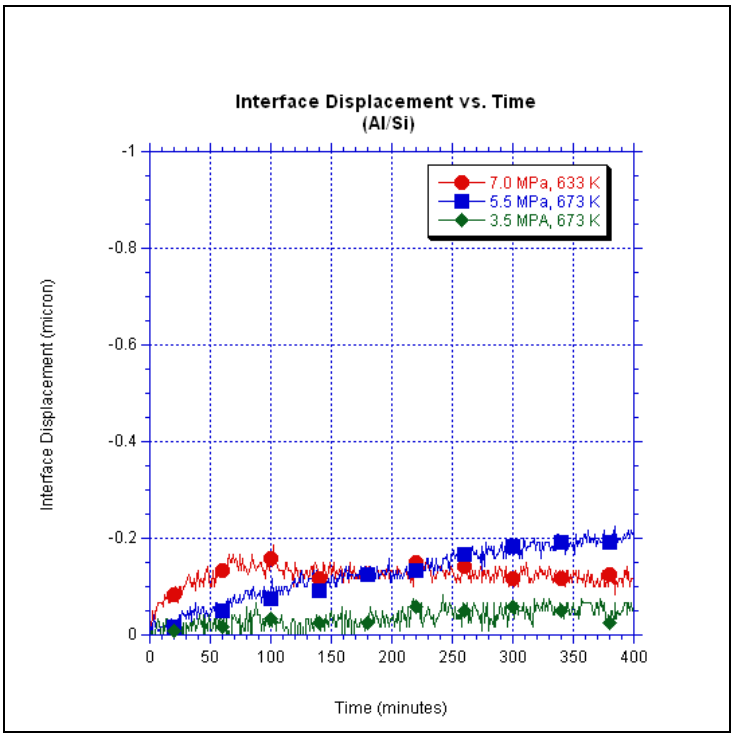

Figure 11 Displacement vs. Time Plots for Al/Si Samples Under Several Conditions

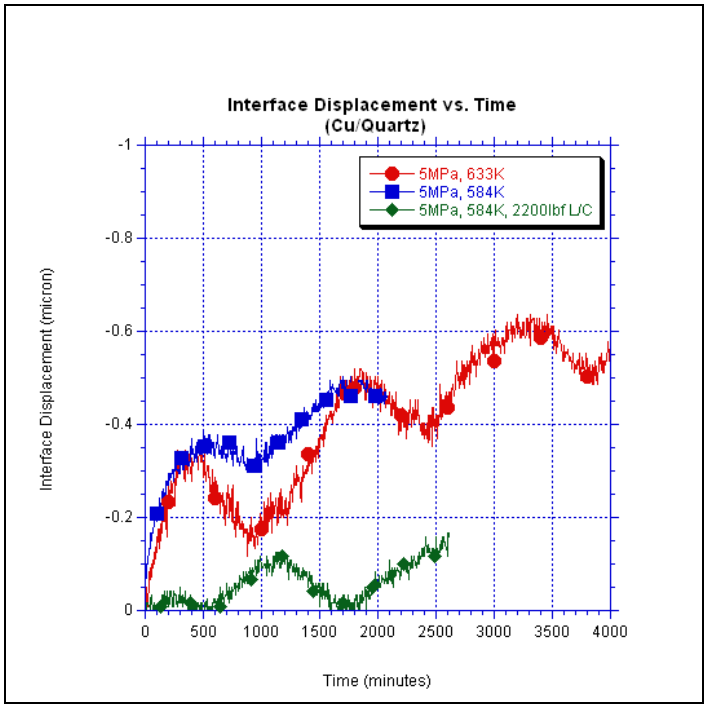

Figure 12 Displacement vs. Time Plots for Cu/Quartz Samples Under Several Conditions

To investigate this oscillation, the sample temperature, load cell temperature, *controlling* load cell load, and *monitoring* load cell load versus time were plotted; see Figures 13 and 14.[1] From Figures 13 and 14, it appears that the periodic oscillations in displacement, load cell temperature, and *monitoring* load cell load are related and that the period of oscillation was nearly 24 hours. The most plausible interpretation of this phenomenon was that throughout the course of a 24 hour period, the laboratory experienced one complete thermal cycle, heating up in the morning and afternoon and cooling in the evening and night. This thermal cycle of the laboratory resulted in an increase in load cell temperature throughout the morning and afternoon and a decrease throughout the evening and night. In response the load cell's zero shifted such that the output signal of the load cell changed in response to changes in the laboratory ambient temperature.

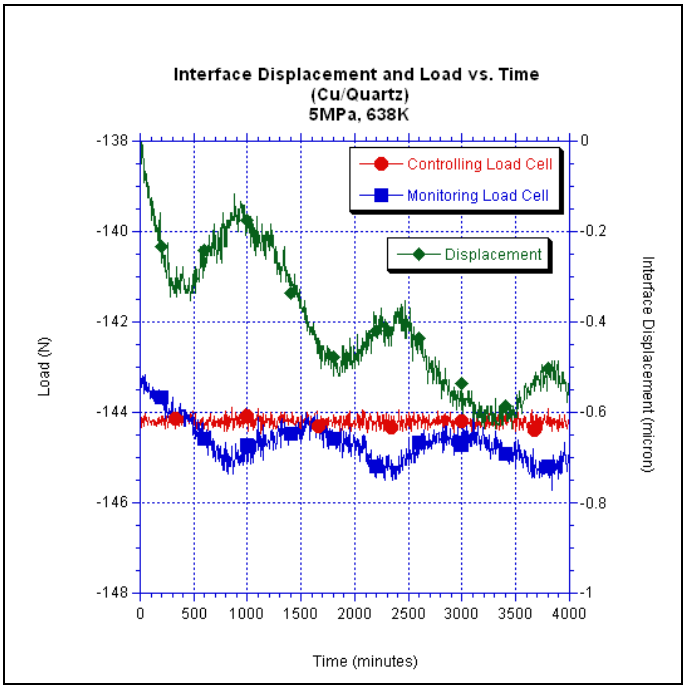

Figure 13 Plots of Interface Displacement and Load vs. Time for a Cu/Quartz Sample

[1] Note that the sample temperature is actively controlled by a temperature feedback controller and the controlling load cell load is also actively controlled by a feedback controller. However, the load cell temperature, displacement, and monitoring load cell load are all free to change and are recorded as received.

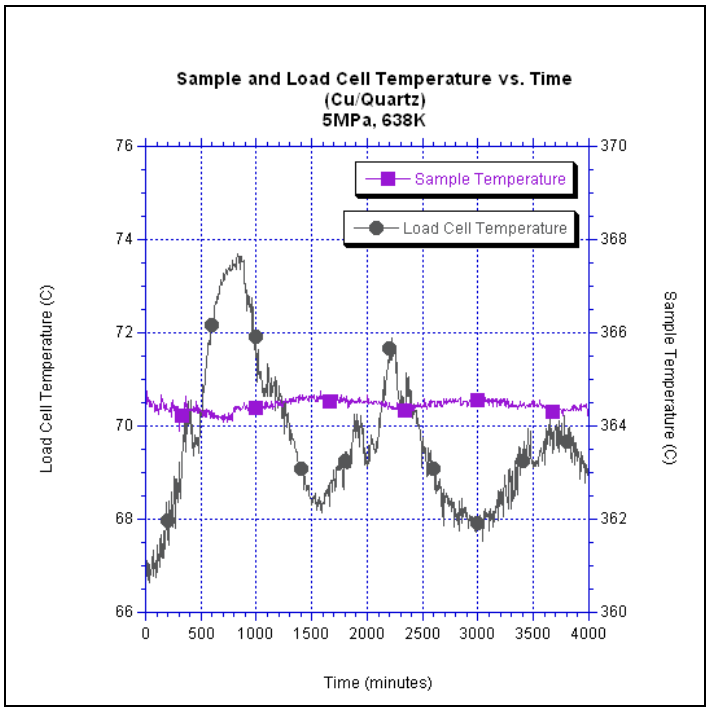

Figure 14 Plots of Sample and Load Cell Temperatures vs. Time for a Cu/Quartz Sample

In Figure 13, the *controlling* load cell load plotted as a flat line depicting a well tuned and well controlled load frame. The *monitoring* load cell on the other hand showed a periodic variation in load with amplitude of as much as +/-0.6N. The difference was that the *controlling* load cell's output signal was used as the feedback signal to the load frame whereas the output signal of the *monitoring* load cell was only used for display. Since the *controlling* load cell was used for feedback, any shift in its zero resulted in the load frame automatically adjusting the applied load to make the *controlling* load cell's output signal match the commanded load. Meanwhile, the *monitoring* load cell's output signal also changed with changing temperature; however, it changed in a different manner than the *controlling* load cell, and as a result, its output reflected the shift in its zero due to temperature as well as changes in the applied load. In other experiments, not plotted here, the roles of the two load cells were swapped and the same type of variation in load was still observed, i.e., one load cell indicated a constant load while the other varied with temperature.

Due to the shift in the load cell zero with temperature and the resultant change in load applied to the specimen, the specimen responded with a small amount of elastic deformation. When the load cell zero shifted such that the applied load increased, the test specimen elastically deformed in compression resulting in an apparent increase in the displacement rate. When the load cell zero shifted such that the applied load decreased, the test specimen elastically recovered resulting in a decrease in the displacement rate.

In order to determine whether the small change in load that would accompany the load cell zero shift was sufficient to provide the level of deformation observed in the creep tests, an experiment was performed in which a Cu/Quartz test specimen was loaded to a nominal stress of 5MPa at room temperature and then the load was varied +/-2.5N about the nominal load using a sine function; see Figure 15. From Figure 15 it is evident that a change in load of 5N resulted in a total change in displacement of about 0.1μm. This amount of deformation was consistent with the variation in displacement seen in the creep tests depicted in Figures 11, 12, and 13.

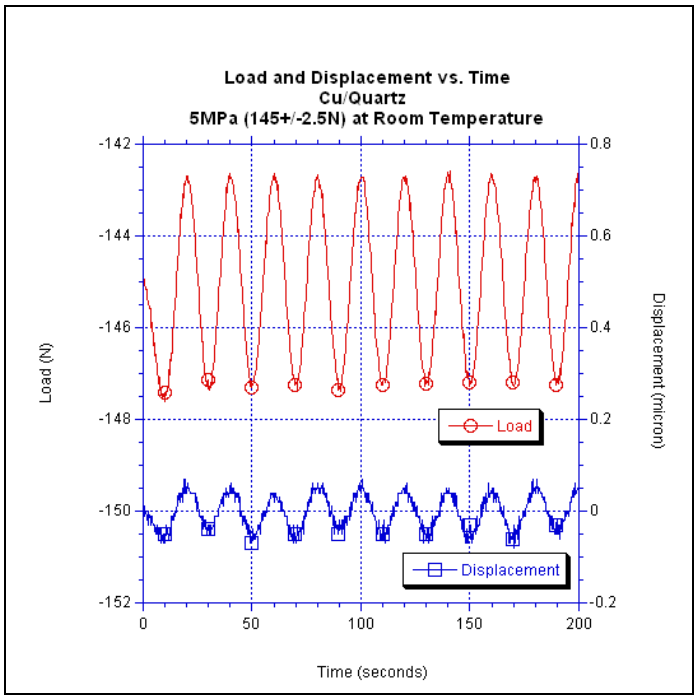

Figure 15 Plots of Load and Elastic Displacement vs. Time for a Cu/Quartz Sample

The load cell used to control load in this study was a Sensotec Model 41 load cell with 500lbf capacity. This particular load cell was temperature compensated, which reduced the sensitivity of the load cell to temperature change; however, according to specifications supplied by the manufacturer it was still possible to incur errors approaching the range of +/-2.5N for the conditions under which the current tests were performed. As a result, it must be assumed that this potential error in loading was present and accounted for a large percentage of the deformation measured in the creep tests.

2. Discussion of Abnormalities

Returning to the sample design explained in the Experimental Procedure chapter above, the aluminum film in the Al/Si samples was incorporated into and constrained by one of the lap shear halves. As a result, the majority of the plastic strain measured in the Al/Si sample was expected to be due to interfacial sliding. In contrast, the Cu/Quartz sample geometry did not incorporate the copper film into either lap shear half and consequently placed less constraint on the copper film. As a result, the plastic strain measured in the Cu/Quartz sample was expected to include not only the effect of interfacial sliding but also the deformation of the bulk of the Cu film. However, the measured deformation was not even as large as predicted for deformation of the bulk of the copper film alone.

According to Frost and Ashby's deformation-mechanism map for pure copper, the test conditions i.e., T = 638K and σ = 7MPa, placed copper in the diffusional flow regime. [23]

The diffusional flow rate equation is: $\dot{\gamma} = \frac{42\sigma_s \Omega}{kTd^2} D_{eff}$ **Equation 4**

Where: $D_{eff} = D_v \left[1 + \frac{\pi \delta D_b}{d D_v} \right]$

$\dot{\gamma}$ is the shear strain rate, σ_s is the shear stress, Ω is the atomic volume, d is the grain size, D_v is the volume diffusion coefficient, D_b is the boundary diffusion coefficient, and δ is the effective thickness of the boundary.

According to Equation 4 and using the parameters for Cu published in Frost and Ashby [23], the steady state strain rate for copper was predicted to be approximately $9.6*10^{-5}$ s^{-1}, which corresponds to a displacement of approximately 8 μm in twenty-four hours for a Cu/Quartz sample.[2] However, the observed displacement was only about 0.6 μm in 72 hours.

One reason for the disparity between the predicted and measured displacement was that the deformation-mechanism map and the diffusional flow rate equation were based on data taken from bulk copper, and may not have been applicable to thin films. Often thin films are found to consist of only a single layer of grains with a preferred orientation. This unique microstructure is significantly different from the typical polycrystalline bulk sample upon which the deformation-mechanism map and rate equation are based. The combined effect of the unique microstructure, the unique lap shear sample geometry, and specimen loading condition may not have produced the necessary potential gradient for significant diffusional flow to occur. As a result very little bulk deformation of the sample was observed.

Why was virtually no interfacial sliding observed? One possible reason was an unexpectedly large interfacial amplitude. Returning to the equation for interfacial sliding:

$$\dot{\bar{U}} \approx K\left[\tau_i + \tau_o\right] \quad \textbf{Equation 3}$$

Where: $$K = \frac{4\delta_i \Omega D_{i_o} e^{\frac{-Q_i}{RT}}}{kTh^2}$$

$$\tau_o = 2\sigma_R \left(\frac{\pi h}{\lambda}\right)^3$$

In the current study, τ_o was taken to be zero, so the displacement rate was given by, $\dot{\bar{U}} \approx K\tau_i$, and therefore the displacement rate was inversely proportional to the

[2] This calculation assumed a grain size of 500nm and temperature of 350°C. Smaller grain sizes are predicted to result in even larger strain rates.

interfacial amplitude squared, $\dot{\bar{U}} \propto \frac{1}{h^2}$. As a result, any change in the interfacial amplitude had a significant effect on the displacement rate.

The fused quartz and silicon substrates used to fabricate test specimens had extremely smooth surfaces prior to sample fabrication. The substrate surfaces were polished to an extremely fine finish. However, in the case of the Al/Si samples, the silicon substrate became severely roughened due to dissolution of silicon into the aluminum film. This phenomenon is described below in the "dissolution, precipitation, and whiskering" section.

In the case of the Cu/Quartz sample there were two separate factors that may have been detrimental to the sliding rate. First, the application of chromium to the surface of the fused quartz to aid in adhesion of the copper film may have significantly increased the apparent interfacial amplitude, *h*, of the sample thereby significantly reducing the sliding rate. Secondly, chromium may have also reduced the diffusivity of the interface such that virtually no sliding could occur. One or both of these factors may have been sufficient to reduce the displacement rate below detectable levels.

B. DISSOLUTION, PRECIPITATION, AND WHISKERING

As stated in the previous section one possible reason interfacial sliding was not observed in the Al/Si samples was that the sample fabrication process caused severe roughening of the silicon substrate surface resulting in a large increase in the interface amplitude, *h*. In order to investigate this roughening, several silicon substrates were coated with Al film and then annealed by heating them to the temperatures the Al/Si samples experienced during diffusion bonding. The surfaces of the annealed Al films were examined using scanning electron microscopy and atomic force microscopy before and after the annealing steps. After annealing and examination, the Al films were removed from the silicon substrates using phosphoric acid. The surfaces of the silicon substrates were examined using SEM and AFM before film deposition and after film removal. The results are given in the paragraphs that follow.

1. Dissolution and Precipitation

Samples for studying the effect of Al on the Si substrate surfaces were fabricated by evaporating 0.75 μm thick Al film on a polished single crystal Si substrate with {100} orientation. Immediately after deposition, the substrates were removed from the deposition chamber and placed in a furnace where they were annealed for two hours in a flowing 98% Ar / 2% H_2 atmosphere. Annealing temperatures ranged from 350^{o}C to 550^{o}C. After annealing, the samples were slowly cooled in the furnace by losses to ambient. After removing the samples from the furnace, the surface of the Al film was examined by SEM and AFM. Later the Al film was removed from the Si substrates by etching with 25wt% H_3PO_4 at 60-70^{o}C.[3] After removing the film the bare Si substrates were again examined by SEM and AFM.

Figures 16 and 17 are SEM micrographs of a Si substrate after the Al film was removed with H_3PO_4. This particular substrate had been annealed at 550^{o}C for 2 hours. The surface of the substrate was uniformly covered with large Si precipitates which were on average 0.6 μm tall. In addition to the large precipitates, the surface of the substrate was also covered with much smaller precipitates, approximately 80 nm in height. These smaller precipitates are not resolved in Figure 16 or 17; they appear as the rough surface in between the large Si precipitates. Figure 18 is a 3-D micrograph produced from the results of an AFM scan of the surface of the same substrate. It depicts the morphology of the smaller precipitates representative of those found between the large precipitates described in Figures 16 and 17. Figure 19 is another micrograph produced from the results of an AFM scan of the surface of the Si substrate with the film removed. Figure 20 is a 2-D profile of the Si Substrate taken from an AFM scan showing the height of the smaller precipitates to be approximately 80 nm and their width to be approximately 300 nm.

[3]It was determined by examining polished Si substrates before and after immersion in 25wt% H_3PO_4 that this acid did not detectably affect the silicon substrate.

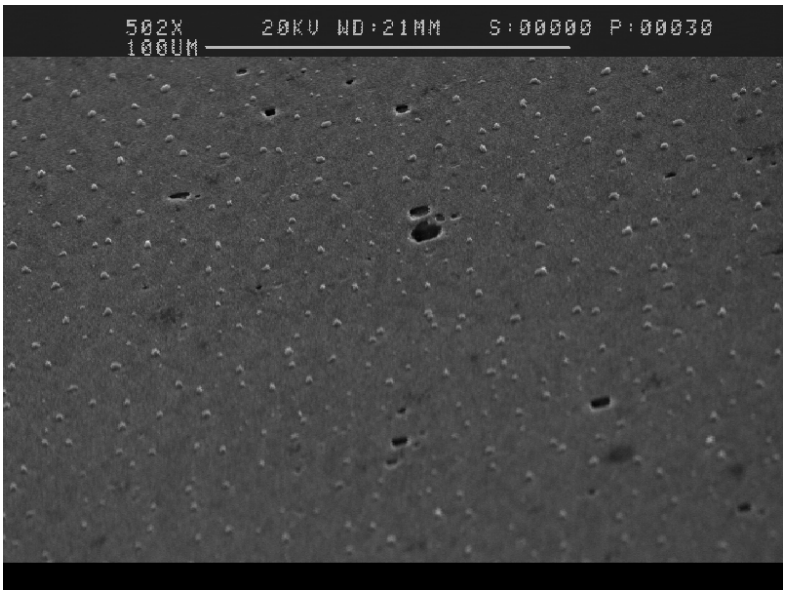

Figure 16 SEM Micrograph of Si Substrate After Annealing at 550^{o}C for 2 Hours. Reveals the Presence of Si Precipitates and Dissolution Pits. (Al Film Removed by Etching with H_3PO_4)

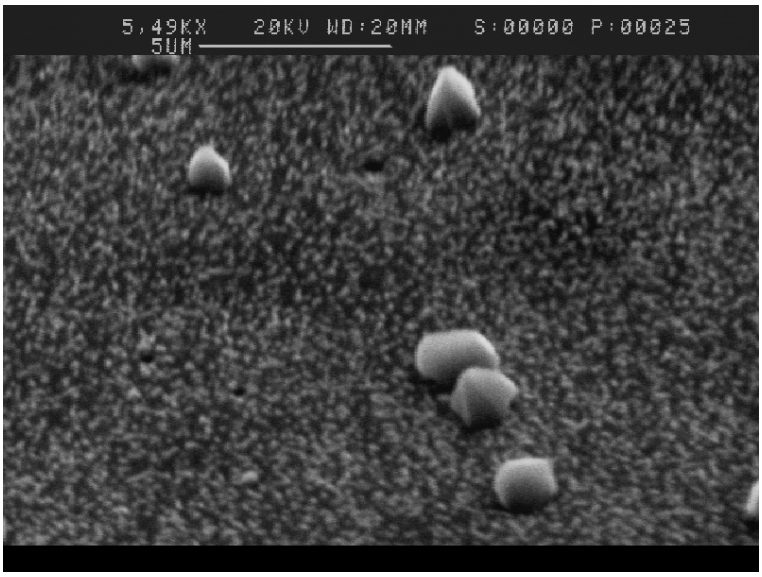

Figure 17 SEM Micrograph of Si Substrate After Annealing at 550^{o}C for 2 Hours. Reveals the Morphology of the "Large" Si Precipitates. "Small" Precipitates Appear as the Rough Surface Between the "Large" Precipitates. (Al Film Removed by Etching with H_3PO_4)

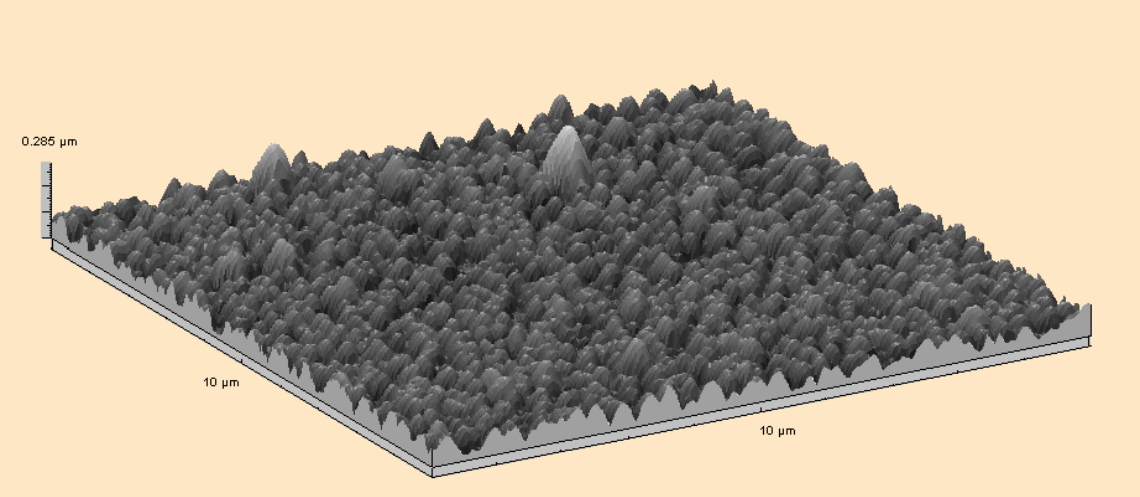

Figure 18 3-D Representation Generated from an AFM Scan of a Si Substrate after Annealing at 550°C for 2 Hours. Reveals the Morphology of the "Small" Si Precipitates. (Al Film Removed by Etching with H_3PO_4)

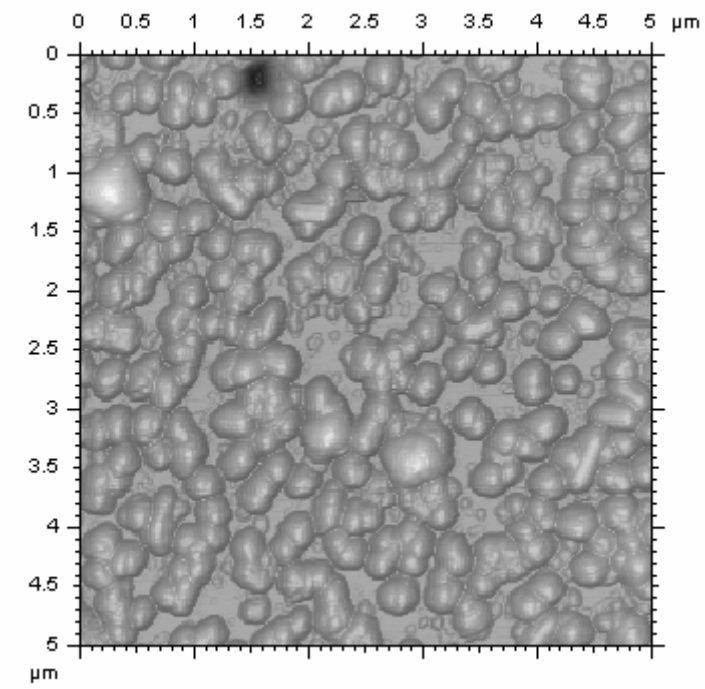

Figure 19 Micrograph Produced from AFM Scan of a Si Substrate Surface after Annealing at 550°C for 2 hours. Reveals the Morphology of the "Small" Si Precipitates. (Al Film Removed by Etching with H_3PO_4)

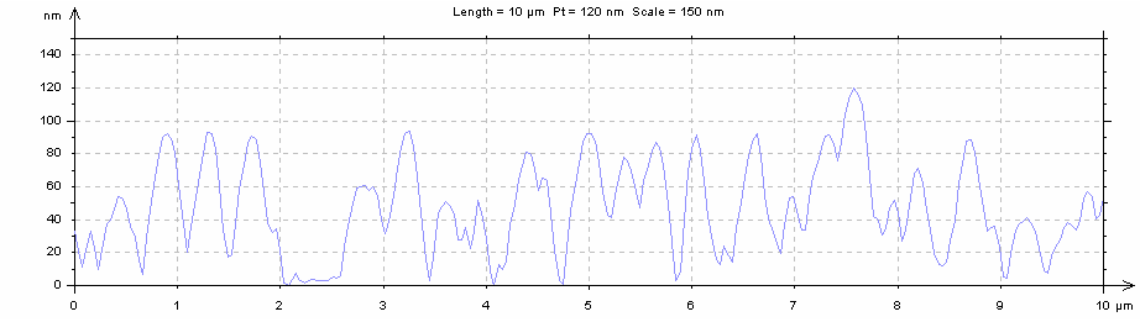

Figure 20 Profile of a Si Substrate after Annealing at 550°C for 2 Hours. Produced from an AFM Scan. (Al Film Removed by Etching with H_3PO_4)

Another feature found on the surface of the Si substrate was dissolution pitting; see Figure 16, the top left in Figure 19, and Figure 21. In Figure 21 the pits appear individually as small dark rectangular areas and clumped together in the three lighter colored circular regions. These pits were caused by selective dissolution of Si by the Al film. Although dissolution of the silicon substrate occurred over the entire interface between the Al and Si, certain areas dissolved faster resulting in pitting of the Si substrate. It is thought that these pits form due to one of three reasons. The first was that a highly defected Al grain overlying the area of pitting more quickly dissolved Si than surrounding grains [24]. The second reason was that selective dissolution occurred in areas where there were imperfections or strain centers in the underlying Si substrate [25]. Consequently the Si crystal was less stable in the area of the strain center and was therefore more susceptible to dissolution. The final reason given for selective dissolution was that prior to depositing the aluminum film, a native silicon oxide layer blanketed the Si substrate and acted as a diffusion barrier between the Si and Al; however, the native silicon oxide layer contained pinholes or imperfections which allowed Al and Si to come into contact. As a result, Si was rapidly dissolved by the Al through these pin holes leaving behind a dissolution pit [26]. The dissolution pits characteristically had rectangular openings corresponding to the {100} orientation of the Si substrate; the sides of the pits were generally faceted.

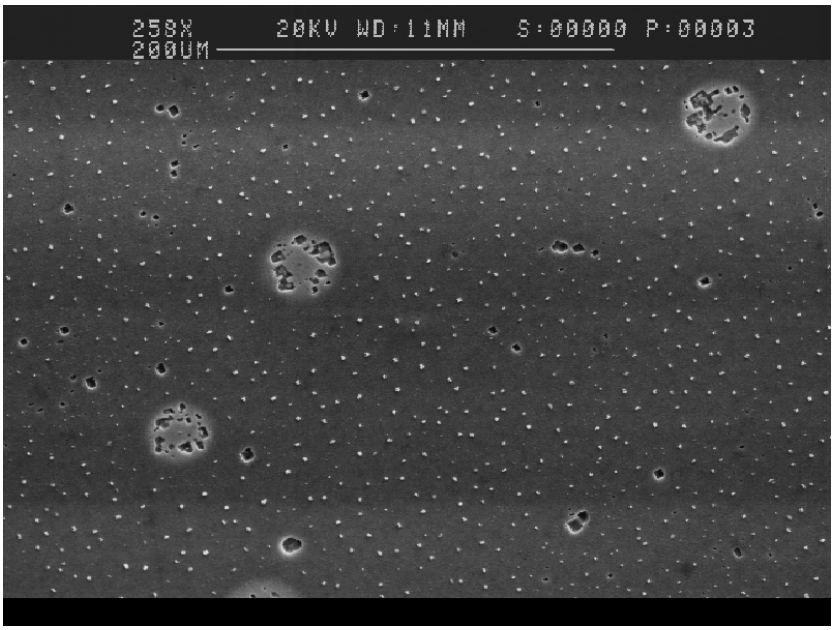

Figure 21 SEM Micrograph of Si Substrate After Anneal at 550^{o}C for 2 Hours. Shows the Distribution of the "Large" Si Precipitates and Dissolution Pits. (Al Film Removed by Etching with H_3PO_4)

The Al-Si phase diagram shows that there is negligible solubility of Si in Al or Al in Si at room temperature. However, at 550^{o}C approximately 1.25at% Si will dissolve in Al, but there is still nearly no Al solubility in Si [27]. Since no diffusion barrier was placed between the Si substrate and Al film, dissolution of Si into the Al film occurred during annealing. Additionally, some areas of the Si substrate dissolved faster than others resulting in pit formation. Upon cooling from the annealing temperature, the Al became supersaturated with Si (owing to the negligible solubility of Al in Si at lower temperature). As a result, relatively pure crystalline Si precipitates nucleated and coarsened in the grain boundaries of the aluminum as well as epitaxially on the remaining Si substrate [24,25,28,29]. Removal of the Al film revealed the underlying precipitates and dissolution pits.

This investigation clearly revealed an extreme change in the surface roughness of silicon substrates as a result of interaction with Al film. The Si surface changed from finely polished to deeply pitted and coated with precipitates. It was hypothesized that similar interfacial roughening due to the dissolution of Si by Al was the main reason

interfacial sliding was not observed in the Al/Si interfacial sliding study. Although the exact morphology of the Si surfaces in the Al/Si interfacial sliding specimens cannot be determined based on this investigation, it can be concluded that dissolution of silicon occurred during the Al/Si interfacial sliding sample fabrication process and resulted in interfacial roughening. It is highly likely that during the diffusion bonding process Si dissolution occurred in the interfacial sliding samples and that upon cooling from the diffusion bonding temperature to room temperature, Si precipitates formed in the Al film. However, since mechanical testing in the interfacial sliding study was conducted at elevated temperature, where Si is somewhat soluble in Al, the same precipitate morphology observed here probably did not also exist in the Al/Si interfacial sliding samples when they were mechanically tested. Regardless of the exact structure of the Al/Si interface in the interfacial sliding samples that evolved, since the interfacial sliding rate is inversely proportional to the square of the interfacial amplitude, the dissolution and pitting of the silicon surface alone could have been significant enough to drive the interfacial displacement rate to zero.

2. Whiskers and Hillocks

In addition to substrate dissolution and silicon precipitation, whiskers and hillocks were found to have grown on the surface of the aluminum film after annealing. The whiskers and hillocks observed were not necessarily important to the interfacial sliding study; however, they were an interesting phenomenon and serve to highlight the extremely high stress that may be induced in a thin film due to coefficient of thermal expansion mismatch. Figures 22 and 23 are SEM micrographs that show typical whiskers that formed on an Al film that was annealed at 427^{o}C for 2 hours. The diameters of the whiskers were generally 1-2 μm, and the lengths were typically between 10 and 20 μm with a few approaching 100 μm or more. The whiskers generally appeared to have faceted surfaces and often showed angular kinks or bends. Figures 24 and 25 are SEM micrographs the show hillocks that formed on the surface of the same Al film. The hillocks generally had a much larger diameter than the whiskers, and they did not display the angular kinks seen in the whiskers.

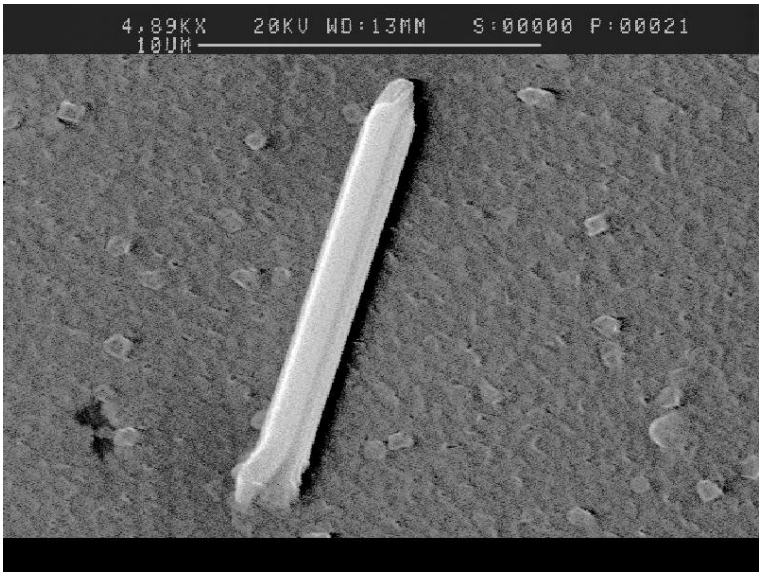

Figure 22 Whisker on the Surface of Al Film Annealed at 427^{o}C for 2 Hours.

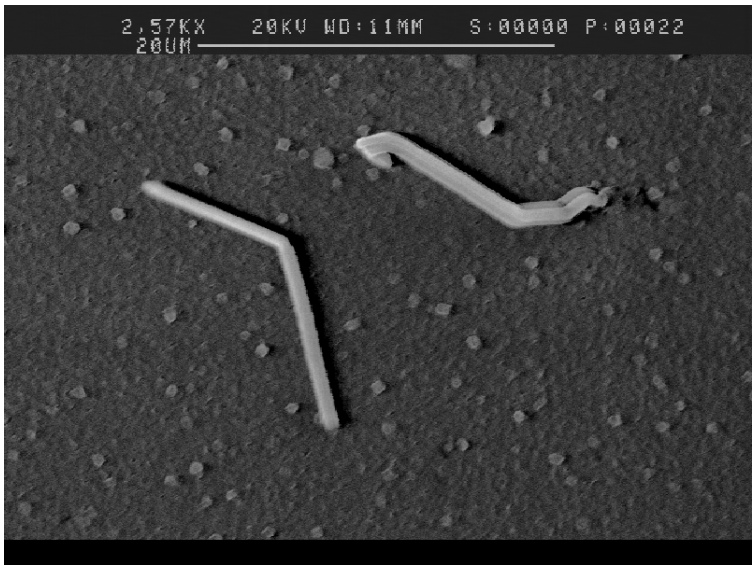

Figure 23 Kinked Whiskers on the Surface of Al Film Annealed at 427^{o}C for 2 Hours.

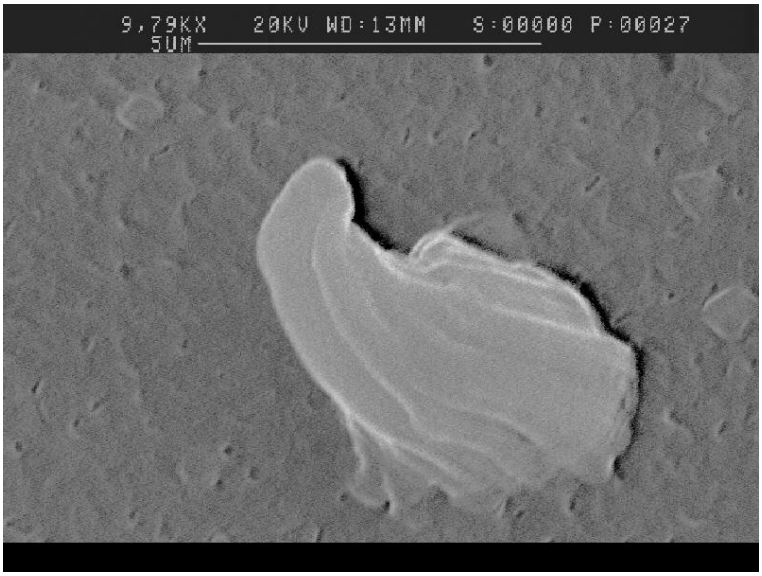

Figure 24 Example of a Hillock on the Surface of Al Film Annealed at 427^{o}C for 2 Hours.

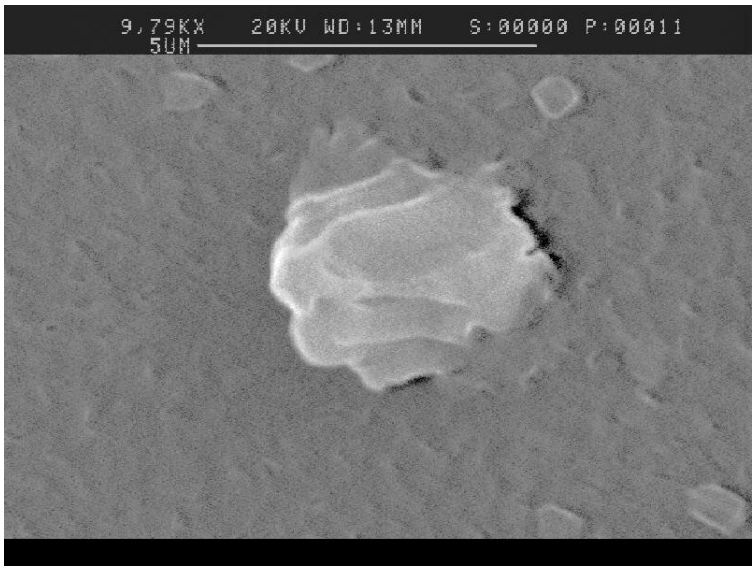

Figure 25 Example of a Hillock on the Surface of Al Film Annealed at 427^{o}C for 2 Hours.

Whisker growth from aluminum films on silicon substrates is a stress relief mechanism that is dependent upon three generally agreed upon requirements; a high homologous temperature, a protective oxide layer, and a compressive stress. The temperature requirement enables rapid self diffusion of Al atoms via grain boundaries

and lattice sites. The surface oxide layer prevents surface diffusion of Al atoms, and the compressive stress gradients serve as the driving force for diffusion within the film.

The compressive stress is typically attributed to differences in thermal expansion between the substrate and Al film [30-35]. Since the coefficient of thermal expansion of aluminum is larger than that of silicon, in-plane compressive stress is induced whenever the temperature of the film and substrate is increased. In metallic thin films other than aluminum, the compressive stresses which give rise to whiskers have also been attributed to intermetallic compound formation [36,37] and to the diffusion and reaction of oxygen in the film [38].

The role of the protective oxide layer is to prevent diffusion of aluminum atoms in response to stress gradients across the free surface of the film. With no oxide layer present Al atoms may diffuse uniformly over the free surface of the film thereby relieving stress in the film with no change in the film surface topography (hillocks or whiskers) [31,32]. If a protective oxide layer is present, diffusion of aluminum over the free surface of the film is much more difficult. As a result, when the film/substrate temperature is increased, compressive stress accumulates in the film until the oxide layer cracks. After the oxide cracks, a whisker is essentially extruded through the crack relieving the stress.

In one model, the protective oxide layer may crack due to elastic deformation of the underlying Al film. Since Al films are often composed of columnar grains with a preferred orientation, when the film is placed in biaxial compression the film's out of plane strain is relatively uniform. However, in areas where grains with abnormal orientations exist, the out of plane strain can be markedly different from surrounding areas resulting in cracks in the oxide layer [37]. These cracks may then serve as a source of vacancies and as a sink for Al atoms allowing diffusion of Al from areas of highest compression to the relatively stress free area in the vicinity of the crack such that a stress free whisker grows out of the crack.

Alternately, as proposed by Eiji Iwamura et al., the oxide layer may become cracked by the diffusion of Al atoms, in response to stress gradients, to specific locations at the interface between the Al film and oxide layer [39]. The accumulation of atoms at

the aluminum/oxide interface stresses the oxide layer until it finally cracks. After the oxide layer cracks, a whisker is essentially extruded from the crack resulting in stress relief of the film.

In conclusion, this study clearly showed the effects of interaction between an aluminum film and a silicon substrate when they were annealed. The silicon substrate surfaces became severely roughened due to dissolution and precipitation. The aluminum film grew whiskers and hillocks in response to the difference in coefficient of thermal expansion. Although the exact morphology of the annealed silicon substrate cannot be extended to the Al/Si samples fabricated for interfacial sliding experiments, it can be concluded that the dissolution and precipitation phenomena observed here also occurred in the Al/Si interfacial sliding samples and that these phenomena increased the interfacial amplitude to such an extent that the sliding rate was driven to zero.

VI. CONCLUSION

Measurement of aluminum thin film sliding on silicon and copper thin film sliding on fused quartz substrates was attempted using a lap shear type of test specimen. Specimen fabrication techniques and testing methodology were developed and refined based on the work done by previous Naval Postgraduate School students. The results of mechanical testing were inconclusive with regard to interfacial sliding. Any sliding that may have occurred during testing was so slow, <0.01μm/hr, that it was deemed essentially undetectable and masked by environmental factors.

Additionally, in the case of Al/Si, the specimen fabrication technique resulted in a highly roughened silicon surface due to silicon dissolution and precipitation in the aluminum film. This highly roughened silicon surface inhibited interfacial sliding such that the Al/Si specimens appeared to be completely non-sliding. In the case of copper and fused quartz, it was necessary to incorporate a thin film of chromium between the copper and quartz in order to increase the adhesion of copper to quartz. The presence of relatively refractory chromium film probably inhibited interfacial sliding by reducing the diffusivity of the interface and by increasing the apparent roughness of the fused quartz.

Further investigation of thin film interfacial sliding should be undertaken in order to better understand the mechanisms and kinetics of interfacial sliding; however, a new approach should be developed. The next steps should include redesign of the test specimen such that the specimen is easier to fabricate and the need to expose the specimen to such severe conditions as required to form diffusion bonds is eliminated. Additionally, the specimen geometry should allow a wider range of stress regime to be tested than the current lap shear geometry which only allows low stress level testing. Finally, the test methodology should be revised such that the test is less sensitive to the laboratory environment.

THIS PAGE INTENTIONALLY LEFT BLANK

LIST OF REFERENCES

1. Gardner, Donald S., and Paul A. Flinn. "Mechanical Stress as a Function of Temperature in Aluminum Films." IEEE Transactions on Electron Devices 35.12 (1988): 2160-2168.

2. Nix, W. D. "Mechanical Properties of Thin Films." Metallurgical Transactions A (Physical Metallurgy and Materials Science) 20A.11 (1989): 2217-2245.

3. Chen, M. W., and I. Dutta. "Atomic Force Microscopy Study of Plastic Deformation and Interfacial Sliding in Al Thin Film: Si Substrate Systems Due to Thermal Cycling." Applied Physics Letters 77.26 (2000): 4298-4300.

4. Park, C., I. Dutta, K. A. Peterson, and J. Vella. "Deformation and Interfacial Sliding in Back-End Interconnect Structures in Microelectronic Devices." Journal of Electronic Materials 32.10 (2003): 1059-1071.

5. Zhmurkin, D. V., T. S. Gross, and L. P. Buchwalter. "Interfacial Sliding in Cu/Ta/Polyimide High Density Interconnects as a Result of Thermal Cycling." Journal of Electronic Materials 26.7 (1997): 791-797.

6. Funn, J. V., and I. Dutta. "Creep Behavior of Interfaces in Fiber Reinforced Metal-Matrix Composites." Acta Materialia 47.1 (1999): 149-164.

7. Raj, R., and M. F. Ashby. "On Grain Boundary Sliding and Diffusional Creep." Metallurgical Transactions 2 (1971): 1113-1127.

8. Peterson, K. A., I. Dutta, and M. W. Chen. "Measurement of Creep Kinetics at Al-Si Interfaces." Scripta Materialia 47.10 (2002): 649-654.

9. Peterson, K. A., I. Dutta, and M. W. Chen. "Diffusionally Accomodated Interfacial Sliding in Metal-Silicon Systems." Acta Materialia 51.10 (2003): 2831-2846.

10. Gross, Todd S., Nazri bin Kamsah, and Igor Tsukrov. "Observation of Heterogeneous, Nanoscale Deformation on Damascene Interconnects with a Polymeric Dielectric." Interconnect Technology Conference, 2001: Proceedings of the IEEE, 2001 International, 2001. 198-200.

11. Zhong, Z. W., K. W. Wong, and X. Q. Shi. "Interfacial Behavior of a Flip-Chip Structure under Thermal Testing." IEEE Transactions on Electronics Packaging Manufacturing 27.1 (2004): 43-48.

12. Huang, M., Z. Suo, and Q. Ma. "Metal Film Crawling in Interconnect Structures Caused by Cyclic Temperatures." Acta Materialia 49 (2001): 3039-3049.

13. Dutta, I., K. A. Peterson, C. Park, and J. Vella. "Modeling of Interfacial Sliding and Film Crawling in Back-End Structures of Microelectronic Devices." IEEE Transactions on Components and Packaging Technology 28.3 (2005): 397-407.

14. Thornell, Mark E. “Sample Fabrication and Experimental Design for Studying Interfacial Creep at Thin Film/Silicon Interfaces.” Master’s Thesis. Naval Postgraduate School, 2004.

15. Parks, C. L. "An Experimental Approach for Studying the Creep Behavior of Thin Film/Substrate Interfaces." Master's Thesis. Naval Postgraduate School, 2004.

16. Sunwoo, Anne. "Diffusion Bonding of Aluminum Alloy, 8090." Scripta Metallurgica 31.4 (1994): 407-411.

17. Dunford, D. V., and P. G. Partridge. "Transient Liquid Phase Diffusion Bonding of 8090 Al-Li Alloy Using Copper Interlayer." Materials Science and Technology 14.5 (1998): 422-428.

18. Huang, Y., F. J. Humphreys, N. Ridley, and Z. C. Wang. "Diffusion Bonding of Hot Rolled 7075 Aluminium Alloy." Materials Science and Technology 14.5 (1998): 405-410.

19. Zuruzi, A. S., H. Li, and G. Dong. "Diffusion Bonding of Aluminium Alloy 6061 in Air Using an Interface Treatment Technique." Materials Science and Engineering A 259 (1999): 145-148.

20. Fujitsuka, Norio, Kanae Hamaguchi, Hirofumi Funabashi, Eishi Kawasaki, and Tsuyoshi Fukada. "Silicon Anisotropic Etching without Attacking Aluminum with Si and Oxidizing Agent Dissolved in TMAH Solution." Sensors and Actuators 114.A (2004): 510-515.

21. Yan, Guizhen, Philip C. H. Chan, I-Ming Hsing, Rajnish K. Sharma, Johnny K. O. Sin, and Yanhyuan Wang. "An Improved TMAH Si-Etching Solution without Attacking Exposed Aluminum." Sensors and Actuators A.89 (2001): 135-141.

22. Brida, S., A. Faes, V. Guarnieri, F. Giacomozzi, B. Margesin, M. Paranjape, G. U. Pignatel, and M. Zen. "Microstructures Etched in Doped TMAH Solutions." Microelectronic Engineering 53 (2000): 547-551.

23. Frost, Harold J., and Michael F. Ashby. Deformation-Mechanism Maps the Plasticity and Creep of Metals and Ceramics. Elmsford, NY: Pergamon Press, 1982.

24. Magee, T. J., and J. Peng. "Si Epitaxial Regrowth and Grain Structure of Al Metallization on <100> Si." Journal of Applied Physics 49.7 (1978): 4284-4286.

25. Fujimura, Norifumi, Hideki Kurosaki, Taichiro Ito, and Yutaka Nakayama. "Dissolution Pits and Si Epitaxial Regrowth in the Al/(111)Si System." Journal of Applied Physics 64.9 (1988): 4499-4502.

26. Rosenburg, R., and M. J. Sullivan. Thin Films-Interdiffusion and Reactions. Eds. J. M. Poate, K. N. Tu and J. W. Mayer: New York: John Wiley and Sons, 1978.

27. Predel, B. Landolt-Bornstein, Group Iv Physical Chemistry - Phase Equilibria, Crystallographic and Thermodynamic Data of Binary Alloys, Volume 5 - Light Metal Structural Alloys. Springer - Verlag. Available: http://www.knovel.com/knovel2/Toc.jsp?BookID=1209&VerticalID=0. May 15 2006.

28. Sankur, H., J. O. McCaldin, and John Devaney. "Solid-Phase Epitaxial Growth of Si Mesas from Al Metallization." Applied Physics Letters 22.2 (1973): 64-66.

29. McCaldin, J. O., and H. Sankur. "Precipitation of Si from the Al Metallization of Integrated Circuits." Applied Physics Letters 20.4 (1972): 171-172.

30. Kim, Deok-kee, Birgit Heiland, William D. Nix, Eduard Artz, Michael D. Deal, and James D. Plummer. "Microstructure of Thermal Hillocks on Blanket Al Thin Film." Thin Solid Films 371 (2000): 278-282.

31. Kim, Deok-kee, William D. Nix, Richard P. Vinci, Michael D. Deal, and James D. Plummer. "Study of the Effect of Grain Boundary Migration on Hillock Formation in Al Thin Films." Journal of Applied Physics 90.2 (2001): 781-788.

32. Chang, C. Y., and R. W. Vook. "The Effect of Surface Aluminum Oxide Films on Thermally Induced Hillock Formation." Thin Solid Films 228 (1993): 205-209.

33. Zaborowski, Michal, and Piotr Dumania. "Kinetics of Hillock Growth in Al and Al-Alloys." Microelectronic Engineering 50 (2000): 301-309.

34. Chaudhari, P. "Hillock Growth in Thin Films." Journal of Applied Physics 45.10 (1974): 4339-4346.

35. Hinode, Kenji, Yoshio Homma, and Yasushi Sasaki. "Whiskers Grown on Aluminum Films During Heat Treatments." Journal of Vacuum Science Technology A 14.4 (1996): 2570-2576.

36. Choi, W. J., T. Y. Lee, K. N. Tu, N. Tamura, R. S. Celestre, A. A. MacDowell, Y. Y. Bong, and Luu Nguyen. "Tin Whiskers Studied by Synchrotron Radiation Scanning X-Ray Micro-Diffraction." Acta Materialia 51 (2003): 6253-6261.

37. Lee, B. Z., and D. N. Lee. "Spontaneous Growth Mechanism of Tin Whiskers." Acta Materialia 46.10 (1998): 3701-3714.

38. Barsoum, M. W., E. N. Hoffman, R. D. Doherty, S. Gupta, and A. Zavaliangos. "Driving Force and Mechanism for Spontaneous Metal Whisker Formation." Physical Review Letters 93.20 (2004): 206104-206101-206104-206104.

39. Iwamura, Eiji, Katsutoshi Takagi, and Takashi Ohnishi. "Effect of Aluminium Oxide Caps on Hillock Formation in Aluminium Alloy Films." Thin Solid Films 349 (1999): 191-198.

INITIAL DISTRIBUTION LIST

1. Defense Technical Information Center
   Ft. Belvoir, Virginia

2. Dudley Knox Library
   Naval Postgraduate School
   Monterey, California